Water Resources Research

RESEARCH ARTICLE
10.1029/2021WR031584

Denitrification-Driven Transcription and Enzyme Production at the River-Groundwater Interface: Insights From Reactive-Transport Modeling

Anna Störiko[1,2], Holger Pagel[3], Adrian Mellage[1,4], Philippe Van Cappellen[5], and Olaf A. Cirpka[1]

[1]Department of Geosciences, University of Tübingen, Tübingen, Germany, [2]Now at Department of Civil and Environmental Engineering, University of Illinois at Urbana-Champaign, Urbana, IL, USA, [3]Biogeophysics, Institute of Soil Science and Land Evaluation, University of Hohenheim, Stuttgart, Germany, [4]Civil and Environmental Engineering, University of Kassel, Kassel, Germany, [5]Department of Earth and Environmental Sciences, Water Institute, University of Waterloo, Waterloo, ON, Canada

Key Points:

- We simulate the distributions of functional-gene transcripts and enzymes related to denitrification at the river-groundwater interface
- Functional-gene transcripts respond quickly to diurnal fluctuations of substrate and oxygen concentrations
- Substrate limitation and oxygen inhibition impede the direct prediction of denitrification rates from transcript or enzyme concentrations

Supporting Information:

Supporting Information may be found in the online version of this article.

Correspondence to:

A. Störiko and O. A. Cirpka,
stoeriko@illinois.edu;
olaf.cirpka@uni-tuebingen.de

Citation:

Störiko, A., Pagel, H., Mellage, A., Van Cappellen, P., & Cirpka, O. A. (2022). Denitrification-driven transcription and enzyme production at the river-groundwater interface: Insights from reactive-transport modeling. *Water Resources Research*, *58*, e2021WR031584. https://doi.org/10.1029/2021WR031584

Received 8 NOV 2021
Accepted 4 AUG 2022

Author Contributions:

Conceptualization: Anna Störiko, Holger Pagel, Adrian Mellage, Philippe Van Cappellen, Olaf A. Cirpka
Data curation: Anna Störiko
Funding acquisition: Olaf A. Cirpka
Methodology: Anna Störiko, Holger Pagel, Adrian Mellage, Olaf A. Cirpka
Software: Anna Störiko
Supervision: Holger Pagel, Philippe Van Cappellen, Olaf A. Cirpka
Visualization: Anna Störiko
Writing – original draft: Anna Störiko

Abstract Molecular-biological data and omics tools have increasingly been used to characterize microorganisms responsible for the turnover of reactive compounds in the environment, such as reactive-nitrogen species in groundwater. While transcripts of functional genes and enzymes are used as measures of microbial activity, it is not yet clear how they are quantitatively related to actual turnover rates under variable environmental conditions. As an example application, we consider the interface between rivers and groundwater which has been identified as a key driver for the turnover of reactive-nitrogen compounds, that cause eutrophication of rivers and endanger drinking water production from groundwater. In the absence of measured data, we developed a reactive-transport model for denitrification that simultaneously predicts the distributions of functional-gene transcripts, enzymes, and reaction rates. Applying the model, we evaluate the response of transcripts and enzymes at the river-groundwater interface to stable and dynamic hydrogeochemical regimes. While functional-gene transcripts respond to short-term (diurnal) fluctuations of substrate availability and oxygen concentrations, enzyme concentrations are stable over such time scales. The presence of functional-gene transcripts and enzymes globally coincides with the zones of active denitrification. However, transcript and enzyme concentrations do not directly translate into denitrification rates in a quantitative way because of nonlinear effects and hysteresis caused by variable substrate availability and oxygen inhibition. Based on our simulations, we suggest that molecular-biological data should be combined with aqueous geochemical data, which can typically be obtained at higher spatial and temporal resolution, to parameterize and calibrate reactive-transport models.

Plain Language Summary Molecular-biological tools can detect how many enzymes, functional genes, and gene transcripts (i.e., precursors of enzyme production) associated with a microbial reaction exist in a sample from the environment. Although these measurements contain valuable information about the number of bacteria and how active they are, they do not directly say how quickly a contaminant like nitrate disappears. Nitrate, from agriculture and other sources, threatens groundwater quality and drinking water production. In the process of denitrification, bacteria can remove nitrate by converting it into harmless nitrogen gas using specialized enzymes. The interface between rivers and groundwater is known as a place where denitrification takes place. In this study, we use a computational model to simulate the coupled dynamics of denitrification, bacteria, transcripts, and enzymes when nitrate-rich groundwater interacts with a nearby river. The simulations yield complex and nonunique relationships between the denitrification rates and the molecular-biological variables. While functional-gene transcripts respond to daily fluctuations of environmental conditions, enzyme concentrations and genes are stable over such time scales. High levels of functional-gene transcripts therefore provide a good qualitative indicator of reactive zones. Quantitative predictions of nitrate turnover, however, will require high-resolution measurements of the reacting compounds, genes, and transcripts.

1. Introduction

Molecular-biological tools and so-called omics techniques, i.e., (meta)genomics, (meta)transcriptomics, (meta)proteomics analyses, have been used to characterize microbial reactions in various environments such as riparian

Writing – review & editing: Anna Störiko, Holger Pagel, Adrian Mellage, Philippe Van Cappellen, Olaf A. Cirpka

zones (Wang et al., 2019), lake and river sediments (Reid et al., 2018; Stoliker et al., 2016), groundwater (Anantharaman et al., 2016; Wegner et al., 2019), and oceans (Louca et al., 2016). They provide information about the microbial community composition, its functional and metabolic *potential* (i.e., genomic data), and *activity* (i.e., transcript data). The continuous developments in extraction and measurement techniques mean that in most natural environments measuring molecular-biological or omics markers is becoming more straightforward than measuring reaction rates. These methods can help to identify the relevant reactive processes at a particular site and the location of reactive zones, and have been hailed as proxies for reaction rates. However, quantitatively relating molecular-biological measurements to the turnover rates of nutrients or contaminants remains a challenge and the validity of the assumption that these are rate-proxies is still in question.

Many sequencing studies target taxonomy and diversity of organisms, without providing direct information about reactions rates. Meta-omics data primarily target the relative abundance of genes, transcripts, and proteins. This semi-quantitative information is particularly difficult to convert into rate expressions. In contrast, measurements of functional genes, their transcripts, and the corresponding enzymes directly relate to the abundance of organisms capable of specific metabolic pathways and their activity. Several studies have suggested using transcript levels or transcript-to-gene ratios to estimate reaction rates of contaminant (Brow et al., 2013; Rahm & Richardson, 2008), pesticide (Monard et al., 2013), or nitrogen-species turnover (Rohe et al., 2020).

Due to the high analytical costs of molecular-biological analyses, highly spatially and temporally resolved measurements of gene, transcript, or enzyme concentrations hardly exist to date. Process-based modeling provides a useful tool with which to bridge between sparse molecular-biological measurements and otherwise highly resolved physical and chemical parameters (e.g., measured using probes), to help validate our conceptual understanding of a system's biological, geochemical, and physical functioning at scales relevant for management. In parallel, such models can also shed light on how transcript and enzyme concentrations relate to reaction rates, and how different factors affect that relationship. A few modeling approaches have been developed that explicitly simulate the levels of transcripts or enzymes, and how they regulate reaction rates, thus, providing a mechanistic link between these variables. For example, Li et al. (2017b) modeled the production of enzymes for denitrification during the incubation of hyporheic-zone sediments using an energetic approach. Song et al. (2017) described the regulation of denitrification enzymes with a cybernetic approach. In the latter, reaction networks are optimized with respect to a metabolic goal such as maximizing the microbial growth rate (Ramkrishna & Song, 2019). Other models feature a mechanistic description of the regulatory chain, including the production of transcription factors triggered by signaling molecules, production of mRNA, and translation into enzymes (Bælum et al., 2013; Koutinas et al., 2011; Störiko et al., 2021). While these approaches provide novel descriptions of enzymatically regulated microbial reactions, there is a lack of studies that analyze how the transport processes that characterize most environmental systems modulate the distributions of functional enzymes.

The microbial nitrogen cycle provides an ideal test case for the development of new modeling approaches that integrate molecular-biological data because the enzymes catalyzing the relevant reaction steps, and the genes coding for them, are relatively well known (Simon & Klotz, 2013). Specific microorganisms use reactive-nitrogen compounds as substrates for redox reactions that fuel their energy metabolism, constituting the main attenuation process for nitrogen contamination in environmental systems (Kuypers et al., 2018). Denitrification is the key reaction for the permanent removal of nitrogen species from the environment because it converts the reactive-nitrogen species nitrate into inert N_2 gas rather than into another reactive-nitrogen species.

We have analyzed the relationship between denitrification rates and transcripts and enzymes in well-mixed systems before (Störiko et al., 2021), but in environmental applications, the reactions are always coupled to transport. Thus, an integrated analysis of the coupled effects of reactions and transport is required to properly assess the applicability of molecular-biological data in more complex settings. The interface between surface waters and groundwater is a good example to study denitrification and its interaction with transport. Hydrologic variations induce dynamic flow regimes, providing an analog for a diverse set of environmental conditions. In addition, the interface is integral at modulating the turnover of nitrogen compounds because steep redox gradients (from oxic rivers to anoxic groundwater) and the availability of labile organic carbon as an electron donor, either in the river water or in the hyporheic and riparian zones, enhance microbial reactions (Krause et al., 2011, 2017).

In this modeling study, we analyze the expected relationships between functional-gene transcripts, enzymes, and genes and denitrification rates in generic surface-water/groundwater systems with contrasting flow dynamics. We

hypothesize that concentrations of transcripts or enzymes in the environment are not a good predictor of reaction rates because several factors may complicate the relationship. For example, enzyme levels can be disconnected from transcript levels due to their different half-lives, and substrate availability, in addition to enzyme levels, regulates the rate of a microbial reaction pathway (Moran et al., 2013; Störiko et al., 2021). Moreover, a meta-analysis of experimental studies pointed out that transcript abundances were not correlated with biogeochemical processes and that it is, therefore, essential to investigate the factors controlling gene abundance, transcription, translation, and enzyme activity to better interpret the patterns of gene and transcript abundances in the environment with respect to ecosystem processes (Rocca et al., 2015).

In our analysis, we apply the current state of knowledge to explore the applicability of molecular-biological data sets as proxies for turnover rates in near-natural settings. By using an enzyme-based reactive-transport model to predict functional-gene transcripts, enzyme concentrations, and denitrification rates, we aim to compare whether predicted transcript and enzyme behavior indeed mirror that of reaction rates, and if not, answer the question of why these differ. We demonstrate the general approach and the associated challenges in the context of denitrification at the river-groundwater interface. Within this example, which we deliberately keep generic, we chose scenarios that differ in potential substrate limitation and dynamics to show their effects on the transcript-rate relationship. While the specific relationships depend on the chosen scenarios and parameter values, we show, via a sensitivity analysis, that the identified patterns are generalizable and unravel factors that determine transcript-rate relations that are transferable to other microbially mediated biogeochemical transformations in environmental systems. Finally, by addressing the challenges related to the quantification of transcripts, enzymes, and reaction rates identified on the grounds of our model results, we provide guidance on how to perform studies that integrate field measurements and modeling, going forward.

2. Methods

2.1. Model Scenarios

We set up three generic model scenarios that represent different hydrological conditions at the river-groundwater interface (Figure 1), ranging from steady-state hydrology and biogeochemistry to pronounced diurnal cycles. None of the scenarios describe a specific site. Instead, they serve as idealized test cases. The differences in biogeochemical and hydrological conditions between the scenarios enabled us to evaluate their impact on simulated transcript and enzyme concentrations and reaction rates. In all scenarios, we considered microbial aerobic respiration and denitrification. Both pathways were coupled to the oxidation of dissolved organic carbon (DOC), released via hydrolysis of particulate organic carbon (POC) in the aquifer matrix and present in the inflowing river water.

The first scenario simulated constant groundwater discharge, where nitrate-rich water from the aquifer discharged into the river (Figure 1a), a common situation in agricultural landscapes. In addition, we assumed that the reactive POC concentration was highest near the river and decreased with increasing distance away from the streambed. That is, we imposed a gradient in the electron donor availability that focused the denitrification activity near the river-aquifer interface. Such spatial patterns in reactive POC are commonly observed in river-groundwater systems where the fresh organic matter trapped in the sediments in direct vicinity of the river is typically considerably more labile than the older POC at greater distance within the aquifer (Krause et al., 2011; Stelzer et al., 2011). The formulation of the gradient is presented in the next section (see Equations 11 and 12).

In the second scenario, we simulated oxic river water continuously entering the aquifer (Figure 1b), mimicking a bank-filtration scenario that could be either induced by pumping or by the natural hydraulic gradient of the system. Oxygen concentrations in river water can be subject to strong daily fluctuations, reflecting the interplay between radiation-dependent photosynthesis, aerobic respiration, and gas exchange in the river (Hayashi et al., 2012; Kunz et al., 2017). We considered two subscenarios: In the first, the oxygen concentration in the river remained at a constant level of 8 mg L^{-1} (bank filtration with constant oxygen), whereas in the second the concentration sinusoidally fluctuated about the mean value, yielding dynamic redox conditions close to the river-groundwater interface (bank filtration with periodic oxygen). Dissolved oxygen levels in real rivers typically show diurnal fluctuations with amplitudes that can vary significantly because of variations in degree of shading, turbidity, nutrient availability, and water depth. The bank-filtration scenario with constant oxygen concentration thus represents the limiting case with a true steady state.

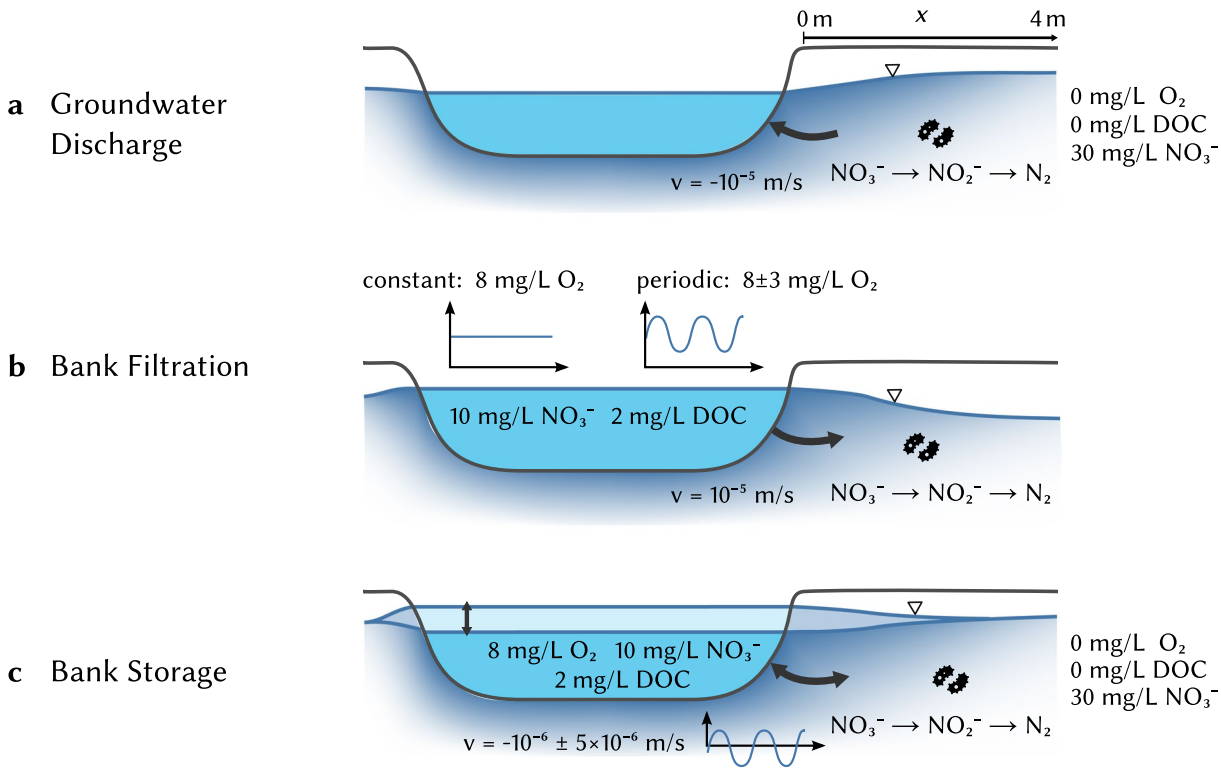

Figure 1. Schematic of the three simulation scenarios and the corresponding boundary conditions. The thick arrow at the river boundary indicates the groundwater flow direction. The inset plots in panel (b) illustrate the oxygen concentration in the river water used for the fixed concentration boundary condition over time. The inset plot in panel (c) illustrates the advective velocity v as function of time.

In a third scenario, denoted bank storage, we considered a flow reversal, induced by dynamic river-stage fluctuations, reflecting, for instance, hydropeaking (Sawyer et al., 2009) or tidal influences (Figure 1c). Close to the river-groundwater interface, the flow reversal caused alternating oxic and anoxic conditions. Although we apply the model to an idealized river-groundwater transitional environment, the general conclusions drawn from this particular setting should more broadly apply to microbially mediated reaction systems in open, natural porous environments.

2.2. Governing Equations

2.2.1. Advective-Dispersive-Reactive Transport

We described transport and reactions of dissolved compounds (nitrate, nitrite, oxygen, DOC) via the one-dimensional (1-D) advection-dispersion-reaction equation. The evolution of compound i's concentration c_i in space (x) and time (t) is thus given by

$$\frac{\partial c_i}{\partial t} + v\frac{\partial c_i}{\partial x} - D\frac{\partial^2 c_i}{\partial x^2} = r^i_{\text{net}}, \tag{1}$$

where v [m s^{-1}] is the average linear flow velocity, D [m^2 s^{-1}] is the dispersion coefficient, and r^i_{net} is the net reaction rate of compound i. We used the parametrization of Scheidegger (1974) for dispersion:

$$D = |v|\alpha_L + D_e, \tag{2}$$

where α_L [m] is the longitudinal dispersivity and D_e [m^2 s^{-1}] denotes the pore-diffusion coefficient. We further assumed that flow is at quasi-steady state, in which v is uniform in space and reacts instantaneously to changes in boundary conditions. In the groundwater-discharge and bank-filtration scenarios, the velocity is constant in time,

whereas in the bank-storage scenario, we approximated v as a sinusoidal function of time with mean velocity $\bar{v}$ [m s^{-1}], amplitude $\hat{v}$ [m s^{-1}] and frequency f_v [s^{-1}]:

$$v(t) = \bar{v} + \hat{v} \sin(2\pi f_v t) \tag{3}$$

In all simulations, we neglected transport of bacterial cells because the majority (>99% according to Griebler et al. (2002)) of active microorganisms in the subsurface are attached to sediments (Smith et al., 2018). Transcripts and enzymes were assumed to be confined to the interior of bacterial cells and thus to be immobile.

2.2.2. Microbial Reactions

We used an enzyme-based model formulation of microbial denitrification (Störiko et al., 2021) that reflects the biological regulation of reaction rates by explicitly simulating concentrations of transcription factors, functional-gene transcripts, and enzymes. The reaction model describes both aerobic respiration and reduction of nitrate to N_2 via NO_2^- as a reactive intermediate. Denitrification is coupled to the oxidation of organic carbon, formally expressed as succinate, serving as an electron donor and carbon source for the facultative anaerobe *Paracoccus denitrificans*. Herein, we applied the parameters of Störiko et al. (2021) specific to *P. denitrificans* to simulate denitrification coupled to DOC oxidation (assuming that succinate acts as a generalized form of DOC) to the flow scenarios outlined in Figure 1. Despite the parameters being specific to a pure-culture batch experiment (Qu et al., 2015), which may not be fully representative for denitrification by the natural microbial community in riverbed sediments, they provide an opportunity with which to probe the thus far poorly characterized behavior of transcription and enzyme regulation in natural subsurface-transport settings, relevant for biogeochemical laboratory and field investigations. In the following, we briefly summarize key model processes and refer the reader to the original publication for more detail.

The catabolic reactions were described by the following stoichiometric equations:

$$7NO_3^- + C_4H_6O_4 \xrightarrow{narG} 7NO_2^- + 4CO_2 + 3H_2O \tag{4}$$

$$14NO_2^- + 14H^+ + 3C_4H_6O_4 \xrightarrow{nirS} 7N_2 + 12CO_2 + 16H_2O \tag{5}$$

$$7O_2 + 2C_4H_6O_4 \longrightarrow 8CO_2 + 6H_2O \tag{6}$$

We chose the *nirS* gene (rather than *norB* or *nosZ*) as the marker gene for the second denitrification step because nitrite but not NO or N_2O accumulated in the lab experiments used for calibrating the model, indicating that nitrite reduction to NO was the rate-limiting step.

For simplicity, denitrification is the only nitrogen-cycling process considered in the model presented here. In natural subsurface environments, such as the river-groundwater system simulated here, the co-occurrence of ammonium and O_2 could activate nitrification, which would then act as another pathway producing nitrite and nitrate. In the absence of O_2, dissimilatory nitrate reduction to ammonium (DNRA) could compete with denitrification for nitrite. While, in principle, the integration of these (and other) additional nitrogen-cycling processes in the model along similar lines as denitrification is possible, currently their parameterization would be seriously hindered by the absence of pertinent observational data.

Gene expression is controlled by the transcription factors FnrP, sensitive to oxygen levels, NarR, regulated by nitrate and nitrite, and NNR, stimulated in the presence of nitrite and absence of oxygen. Transcription of the *narG* gene, coding for nitrate reductase (NAR), is initiated in the presence of FnrP and NarR, whereas the transcription of *nirS*, coding for nitrite reductase (NIR), requires NNR. The concentrations of transcripts were assumed to be at quasi-steady state with the transcription factor concentrations. The NAR and NIR enzymes are produced in response to *narG* and *nirS* levels and decay following a first-order rate (Störiko et al., 2021).

Denitrification rates are a function of the enzyme concentrations, a double Michaelis-Menten term for the limitation of electron-donor (DOC) and electron-acceptor (nitrate, nitrite) concentrations and an oxygen inhibition term:

$$r_N = k^j_{\max} E_j \frac{c_N}{K_N + c_N} \frac{c_{\mathrm{DOC}}}{K_{\mathrm{DOC}} + c_{\mathrm{DOC}}} \frac{I^j_{\mathrm{O}_2}}{c_{\mathrm{O}_2} + I^j_{\mathrm{O}_2}} \tag{7}$$

Here, $k^j_{\max}$ [s^{-1}] is the amount of substrate that the enzyme j (NAR or NIR) can maximally turn over per time (also called turnover number), E_j [mol L^{-1}] is the concentration of enzyme j that catalyzes the reaction of substrate N (nitrate or nitrite). K_N [mol L^{-1}] and K_{DOC} [mol L^{-1}] are the half-saturation concentrations for nitrate/nitrite and DOC, respectively, and $I^j_{\mathrm{O}_2}$ [mol L^{-1}] is the oxygen inhibition constant for enzyme j.

Aerobic respiration was described by a standard double Michaelis-Menten formulation with the maximum cell-specific respiration rate $v^{\mathrm{O}_2}_{\max}$ [mol $cell^{-1}$ s^{-1}] and biomass concentration B [cells L^{-1}]:

$$r_{\mathrm{O}_2} = v^{\mathrm{O}_2}_{\max} B \frac{c_{\mathrm{O}_2}}{K_{\mathrm{O}_2} + c_{\mathrm{O}_2}} \frac{c_{\mathrm{DOC}}}{K_{\mathrm{DOC}} + c_{\mathrm{DOC}}} \tag{8}$$

To predict the dynamics of transcripts and enzymes under conditions similar to those found in natural environments, we modified and complemented the parts of the model that relate to DOC and biomass. Here, the model was expanded to include the release of DOC from POC in the aquifer matrix, and its consumption by both denitrification and aerobic respiration. The latter yielded a DOC consumption dependent on the electron-acceptor consumption rates (defined in Equations 7 and 8) and their stoichiometric coefficients in the metabolic reaction:

$$r^j_{\mathrm{DOC}} = \frac{\gamma^i_{DOC}}{\gamma^j_A} r^j_A \tag{9}$$

and

$$r_{\mathrm{DOC}} = \sum_j r^j_{\mathrm{DOC}}, \tag{10}$$

where γ^j_A and γ^j_{DOC} are the stoichiometric coefficients of the electron acceptor and DOC in reaction j and r^j_A is the corresponding electron-acceptor reaction rate. We modeled the release of DOC from the POC-containing aquifer matrix as a first-order mass transfer process (Gu et al., 2007; Kinzelbach et al., 1991; Knights et al., 2017), with the first-order coefficient $k^{\mathrm{DOC}}_{\mathrm{release}}$ [1/s]:

$$r_{\mathrm{release}} = k^{\mathrm{DOC}}_{\mathrm{release}} \left(c^{\mathrm{sat}}_{\mathrm{DOC}} - c_{\mathrm{DOC}} \right) \tag{11}$$

The DOC saturation concentration $c^{\mathrm{sat}}_{\mathrm{DOC}}$ [mol L^{-1}] depends on the POC content of the sediment, which tends to decrease with distance from the river (Marmonier et al., 1995; Stelzer et al., 2011). Following Knights et al. (2017), we therefore assumed an exponential profile of $c^{\mathrm{sat}}_{\mathrm{DOC}}$:

$$c^{\mathrm{sat}}_{\mathrm{DOC}} = c^{\mathrm{sat},0}_{\mathrm{DOC}} \exp\left(-\frac{x}{l}\right), \tag{12}$$

where l [m] is the length scale parameter for the concentration decrease (Table 1).

In contrast to the original formulation, bacterial growth was parameterized as a function of the oxidation of organic carbon coupled to both oxygen and nitrogen oxide reduction. The synthesis of biomass, represented with the molecular formula $C_{10}H_{18}O_5N_2$, can formally be described by the reaction

$$3C_4H_6O_4 + 2NH^+_4 \longrightarrow C_{10}H_{18}O_5N_2 + 2CO_2 + 3H_2O + 2H^+ \tag{13}$$

$NH_4{}^+$ is assumed to be nonlimiting for microbial growth, and is not explicitly simulated. Equation 13 was then coupled to the energy-gaining reactions (Equations 4–6) to obtain the overall metabolic reaction. The stoichiometric coefficients in the metabolic reaction depend on the number of catabolic formula reactions that must be completed to generate the energy required for one anabolic formula reaction (and thus produce one mole of biomass). In turn, this number is directly related to the growth yield Y_i [cells (mol C)$^{-1}$], which corresponds to the

Table 1
Parameter Values Used in the Simulation

Parameter	Description	Value	Unit	Reference
Transport parameters				
v	Linear velocity[a]	10^{-5}	m s^{-1}	b
$\bar{v}$	Mean velocity[c]	-10^{-6}	m s^{-1}	d
$\hat{v}$	Velocity amplitude[c]	10^{-5}	m s^{-1}	d
f_v	Velocity frequency[c]	1	d^{-1}	e
α_L	Longitudinal dispersivity	0.1	M	f
D_e	Effective diffusion coefficient	3×10^{8}	m^2 s^{-1}	g
Reaction parameters				
$k_{max}^{NO_3^-}$	NAR turnover number	4.4×10^{4}	s^{-1}	h
$k_{max}^{NO_2^-}$	NIR turnover number	2.9×10^{2}	s^{-1}	h
$K_{NO_3^-}$	NO_3^- half-saturation constant	5	μM	i
$K_{NO_2^-}$	NO_3^- half-saturation constant	5	μM	i
K_{DOC}	DOC half-saturation constant	40	μmol C L^{-1}	j
$I_{O_2}^{NAR}$	O_2 inhibition constant for NAR	1	μM	h
$I_{O_2}^{NIR}$	O_2 inhibition constant for NIR	340	nM	h
$\nu_{max}^{O_2}$	Maximum cell-specific O_2 oxidation rate	6.4×10^{-19}	mol cell^{-1} s^{-1}	h
K_{O_2}	O_2 half-saturation constant	31	μM	h
$k_{release}^{DOC}$	DOC release rate constant	0.2	d^{-1}	k
$c_{DOC}^{sat,0}$	Maximum DOC saturation concentration	20.8	mmol C L^{-1}	l
L	length scale for decrease in sediment POC	0.2	m	m
$Y_{max}^{NO_3^-}$	Maximum growth yield with NO_3^-	2.6×10^{13}	cells (mol C)$^{-1}$	n
$Y_{max}^{NO_2^-}$	Maximum growth yield with NO_2^-	1.6×10^{13}	cells (mol C)$^{-1}$	n
$Y_{max}^{O_2}$	Maximum growth yield with O_2	7.7×10^{13}	cells (mol C)$^{-1}$	h, o
B_{max}	Carrying capacity	3.3×10^{11}	cells L^{-1}	p
k_{dec}	Biomass decay constant	10^{-7}	s^{-1}	q
Boundary conditions				
$c_{O_2}^{in}$	O_2 concentration in the river[r]	250	μM	s
$\overline{c_{O_2}}$	Mean O_2 concentration in the river[t]	250	μM	s
$\widehat{c_{O_2}}$	Amplitude of oxygen fluctuations[t]	94	μM	u
$c_{NO_3^-}^{river}$	NO_3^- concentration in the river	161	μM	v
$c_{NO_3^-}^{GW}$	NO_3^- concentration in groundwater	484	μM	v
c_{DOC}^{river}	DOC concentration in the river	167	μmol C L^{-1}	w

[a]Groundwater-discharge and bank-filtration scenarios. [b]See Bertin and Bourg (1994) for bank filtration and Kennedy et al. (2009) for groundwater exfiltration. [c]Bank-storage scenario. [d]Gerecht et al. (2011) and Liu et al. (2017). [e]Diurnal cycles. [f]Gelhar et al. (1992). [g]Based on the approximation $D_e = D\theta$ where $D = 10^{-9}$ m^2 s^{-1} is the molecular diffusion coefficient and $\theta = 0.3$ is porosity. [h]Median of the parameters in Störiko et al. (2021). [i]Hassan et al. (2016). [j]Fixed to a value within reported ranges (Kinzelbach et al., 1991; Sanz-Prat et al., 2016). [k]Fixed to a value within reported ranges (Gu et al., 2007; Kinzelbach et al., 1991; Sanz-Prat et al., 2016; Sawyer, 2015). [l]Fixed to a value within reported ranges (Gu et al., 2007; Kinzelbach et al., 1991; Sawyer, 2015). [m]Knights et al. (2017). [n]Fixed to a value within reported ranges (Hassan et al., 2014, 2016). [o]Value corrected for the incorporation of organic carbon into biomass, which was not considered in Störiko et al. (2021). [p]Fixed to a value within reported ranges (Ding, 2010). [q]Fixed to a value within reported ranges (Ding, 2010; Kinzelbach et al., 1991). [r]Groundwater-discharge, bank-storage, and bank-filtration scenarios with constant oxygen. [s]Liu et al. (2017). [t]Bank-filtration scenario with fluctuating oxygen. [u]Kunz et al. (2017). [v]Gu et al. (2007) and Liu et al. (2017). [w]Hayashi et al. (2012), Bol et al. (2015), and Thurman (1985).

amount of biomass that is produced per mole of organic carbon consumed. The growth yield relates the growth rate associated to the electron acceptor i to the corresponding DOC-consumption rate:

$$r^i_{\text{growth}} = Y_i r^i_{\text{DOC}} \tag{14}$$

Furthermore, we applied a logistic term to the biomass-growth expression (not to the substrate consumption rates) to limit biomass growth to a set maximum density (e.g., Grösbacher et al., 2018). This is in line with observations that biomass densities in porous media reach a "carrying capacity," even under nongrowth-limiting conditions (Ding, 2010; Mellage et al., 2015). The logistic growth term can be interpreted as a reduction in the maximum growth yield by the occupancy level:

$$Y_i = Y^i_{\text{max}} \left(1 - \frac{B}{B_{\text{max}}}\right), \tag{15}$$

where Y^i_{max} is the maximum growth yield and B_{max} is the carrying capacity. This implies that the growth yield and therefore the stoichiometric coefficients of the metabolic reactions depend on the biomass concentration. The model also accounts for biomass decay via a first-order term with the decay coefficient k_{dec} [s^{-1}]:

$$r_{\text{decay}} = k_{\text{dec}} B, \tag{16}$$

leading to the build-up of dead biomass, which, in turn, decays in a first-order process with constant k_{min}, releasing DOC via mineralization.

2.2.3. Boundary Conditions

Fixed concentration (Dirichlet) boundary conditions were applied at the river and groundwater-inflow boundaries. The river water was assumed to be saturated with respect to oxygen, and contained 10 mg L^{-1} of nitrate and 2 mg L^{-1} of DOC. These concentrations correspond to anthropogenically influenced but not excessively eutrophic rivers. The inflowing groundwater was assumed to be anoxic but rich in nitrate (30 mg L^{-1}) and depleted in DOC. The DOC concentrations were chosen based on meta-studies showing that DOC levels in groundwater are generally low whereas river water DOC concentrations tend to be higher (McDonough et al., 2020; Thurman, 1985). In the bank-filtration scenario with fluctuating oxygen levels, the oxygen concentration in the river was described by a sinusoidal function with amplitude $\widehat{c_{O_2}}$ [mol L^{-1}], frequency $f_{O_2} = 1$ day^{-1} and mean value $\overline{c_{O_2}}$ [mol L^{-1}]:

$$c^{\text{in}}_{O_2}(t) = \widehat{c_{O_2}} \sin\left(2\pi f_{O_2} t\right) + \overline{c_{O_2}} \tag{17}$$

All other concentrations at the inflow boundary were constant over time, with values given in Table 1. At the outflow boundary, we assumed zero dispersive flux.

2.3. Simulation Parameters

Parameters related to transcript and enzyme concentrations, denitrification and aerobic respiration were obtained from our previous study (Störiko et al., 2021) in which we calibrated the enzyme-based model with the laboratory data of Qu et al. (2015). In the simulations presented here, the median values of the parameter distributions in Störiko et al. (2021) were imposed (Table 1). Values of new parameters, i.e., those that were not included in the previous model (transport and DOC-related parameters) were chosen based on literature values.

2.4. Sensitivity Analysis

We conducted a local sensitivity analysis that assessed the impact of reaction parameters on simulation results and, in a second step, identified influential reaction parameters by computing the principal components of parameter sensitivities. After determining the most sensitive parameter values, we analyzed their influence on our modeling results by model runs in which the most sensitive parameters were modified.

Local parameter sensitivities were normalized to the reference parameter values such that they correspond to the sensitivities of the outputs with respect to the log parameters. The normalized sensitivity s_{ij} of output f_i with respect to parameter p_j is given by

$$s_{ij} = \frac{\partial f_i(\mathbf{p})}{\partial p_j} p_j = \frac{\partial f_i(\exp \mathbf{q})}{\partial q_j} \tag{18}$$

where $q_j = \ln(p_j)$. We approximated the sensitivities via direct numerical differentiation

$$s_{ij} \approx \frac{\Delta_j f_i}{\Delta p_j} p_j \approx \frac{f_i(\exp(\mathbf{q} + \Delta_j \mathbf{q})) - f_i(\exp \mathbf{q})}{\Delta q_j} \tag{19}$$

where entry k of the vector $\Delta_j \mathbf{q}$ is defined by

$$(\Delta_j q)_k = \begin{cases} \Delta q_j & \text{if } k = j, \\ 0 & \text{otherwise.} \end{cases} \tag{20}$$

We define

$$\Delta q_j = \log(1 + \alpha), \tag{21}$$

where α is a small relative perturbation of the parameters that we chose to be 1%.

We computed sensitivities for all concentrations and the denitrification rates. Sensitivities were normalized by the spatial integral of each respective parameter, enabling a cross-comparison of parameter sensitivities with differing magnitudes.

$$s_{ij}^{\text{norm}} = \frac{s_{ij}}{\int_0^L f_i(x)\mathrm{d}x}, \tag{22}$$

where $L = 4$ m is the length of the domain.

For each scenario, we conducted a principal component analysis (PCA) of the sensitivity matrix (of size $(n_{\text{species}}\, n_x) \times n_{\text{parameters}}$ in the steady-state scenarios and $(n_{\text{species}}\, n_x\, n_t) \times n_{\text{parameters}}$ in the time-variable bank-storage scenario) to identify parameter combinations that explain the (co-)variance of sensitivities in space and across concentrations of different species.

2.5. Numerical Methods

We used the cell-centered finite volume method to discretize the reactive-transport Equation 1 in space, applying a first-order upwind scheme for advection. The domain had a total length of 4 m and was divided into 200 cells with a uniform spacing of 2 cm. The resulting system of ordinary differential equations (ODEs) was solved with the backwards differentiation formula (BDF) as implemented in the CVODES solver in the SUNDIALS library (Hindmarsh et al., 2005). All code was written in Python 3.8, and the package Sunode (Seyboldt, 2021) that wraps CVODES was used for solving the ODEs. The simulations were run until reaching steady state (in the scenarios with constant boundary conditions) or dynamic steady state, that is, self-repeating time cycles in the scenarios with periodic boundary conditions.

3. Results

3.1. Zonation of Redox Species and Denitrifying Bacteria

The three model scenarios result in distinct spatial distributions of nitrogen species, transcripts, enzymes, biomass, oxygen, and DOC (Figure 2, rows a–f). In the following, we present and discuss the predicted steady-state concentrations scenario-wise in detail: groundwater discharge (Figure 2, left column), bank filtration (Figure 2, center column), and bank storage (Figure 2, right column).

3.1.1. Scenario Groundwater Discharge

Nitrate enters the domain with inflowing groundwater, and remains at high concentrations (i.e., close to the inflow value) over the first 2 m of the domain, where the aquifer matrix contains only little POC (electron donor

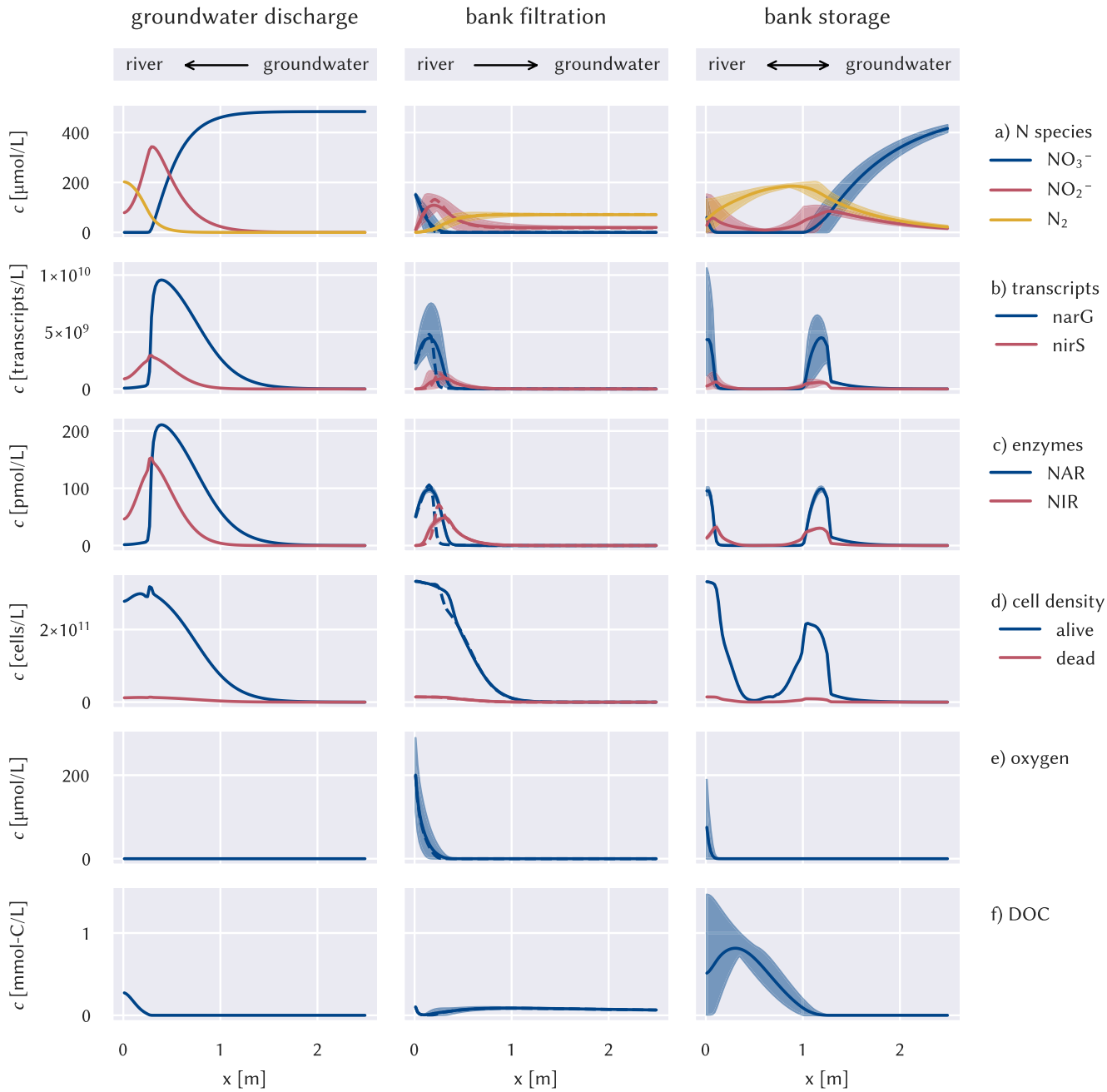

Figure 2. Spatial distributions of nitrogen compounds (a), transcript (b) and enzyme (c) concentrations, biomass (d), oxygen (e), and dissolved organic carbon (DOC) (f) in the different scenarios. The steady-state solution in bank-filtration scenario with constant oxygen input is indicated by a dashed line. For the periodic solution in bank-filtration scenario with periodic oxygen input and the bank-storage scenario, the minimum and maximum values over time are indicated by the shaded area, the mean value is plotted as a solid line. Concentrations between 2.5 m and the groundwater-side domain boundary at 4 m are omitted because they are almost constant.

limitation). At about 1.5 m from the river, nitrate begins to drop and is completely depleted at a distance of 0.25 m from the sediment-river interface. Nitrite concentrations increase, mirroring the drop in nitrate, until reaching a peak value of 340 µmol L^{-1} at 0.3 m and then decrease toward the river. Our model-predicted nitrite concentrations are higher than typically observed in natural sediments. Profiles of pore-water nitrite in several studies indicate that the concentrations are usually below 30 µmol L^{-1} (Akbarzadeh et al., 2018; Harvey et al., 2013; Stief et al., 2002). The parameter set used here is based on laboratory batch experiments with a single strain where strong nitrite accumulation was observed (Störiko et al., 2021). Thus, the high model-derived nitrite concentrations are likely a feature specific for the microbial strain used in the experiments.

The concentration of DOC drops from 280 µmol C L^{-1} at the sediment-river interface to below 40 nmol C L^{-1} within 30 cm, driven by the prescribed exponentially decreasing content of POC in the sediment (the only source of DOC) away from the river boundary. The zones of nitrate and nitrite consumption coincide with elevated absolute concentrations of *narG* and *nirS* transcripts (i.e., in units of transcripts L^{-1}) and NAR/NIR enzymes (Figure 2c, left column). In contrast, cell-specific *narG* transcript and NAR enzyme concentrations are high in the DOC-limited section of the domain, despite the absence of denitrification (Figure S1 in Supporting Information S1). Nitrate triggers transcription but the low availability of the electron donor (DOC) yields low biomass concentrations, strongly limiting denitrification. High biomass concentrations are only reached close to the river, where the denitrification activity is the highest.

3.1.2. Scenario Bank Filtration

The center column in Figure 2 shows the dynamics of the two bank-filtration scenarios with periodic and constant oxygen concentrations in the inflow. In the periodic bank-filtration scenario, concentrations do not reach a steady state but concentration time series converge to repeating diurnal cycles (often denoted *dynamic steady state*).

The model predicts a zonation of the redox processes starting with aerobic respiration at the inflow boundary, where oxygen-rich river water infiltrates. Nitrate, present in the incoming water, is subsequently reduced to nitrite and N_2. The fluctuating oxygen concentrations in the river (inflow) in the bank-filtration scenario leads to a periodic shift in the location of the denitrification zone, which oscillates back and forth over 0.1 m about 0.2 m, as indicated by the position of the nitrite peak. At a given location, nitrate and nitrite concentrations fluctuate considerably over the course of the day. For example, nitrate concentrations at 0.2 m vary between 60 µmol L^{-1} and total depletion. Nitrite is reduced to low, but nonzero "residual" concentrations (20 µmol L^{-1}). The low concentration front subsequently penetrates deep into the aquifer.

Biomass concentrations are very stable over time in the scenario with a fluctuating inflow oxygen concentration and hardly differ from the scenario with constant oxygen input. Cell doubling times in the simulations range from a few hours to several days, which is in accordance with literature values (Mailloux & Fuller, 2003). Similarly, biomass decay is slow (with a half-life of about 80 days, see Table 1), such that the biomass does not respond to daily cycles of substrate availability. Biomass concentrations are highest at the river-inflow boundary where neither oxygen nor DOC are limiting and cell densities reach the maximum capacity B_{max}. At locations where oxygen and nitrate are consumed, the remaining low nitrite concentrations can only sustain the survival of a small biomass pool (starting at 1.3 m from the river boundary), which in turn reduces the denitrification rate to values close to zero.

Transcripts of the *narG* gene are abundant in the region where nitrate is available and *nirS* transcripts co-occur with nitrite. In the scenario with dynamic boundary conditions, the transcript concentrations of denitrification genes exhibit a distinct diurnal cycle with an amplitude of up to 70% (*narG*) and 100% (*nirS*) of the mean value, in some parts of the domain. Concentrations of NAR and NIR enzymes follow the patterns of *narG* and *nirS* transcripts, but are much more dampened, with amplitudes that are 1 order of magnitude smaller than those of the corresponding transcripts. This difference stems from the different time scales of production and decay of transcript and enzymes. While transcripts usually decay within a few minutes (Bernstein et al., 2002; Härtig & Zumft, 1999) and are therefore assumed to be at quasi-steady state in our simulations, enzyme half-lives range on the order of several hours to days (Maier et al., 2011).

Because of the high DOC concentration (0.1 mmol L^{-1}) imposed at the river boundary, the river water serves as a DOC source. The DOC concentration, however, drops sharply in the aquifer due to the high microbial electron-donor demand, driven by the presence of oxygen and nitrate. Outside of the zone of denitrification, the DOC concentration rises toward the groundwater boundary, driven by the hydrolysis of POC, reaching a maximum at about 1 m. The decreasing POC content away from the river yields a final gradual decline in DOC approaching the groundwater boundary.

3.1.3. Scenario Bank Storage

In the bank-storage scenario, the alternating inflow of nitrate from the aquifer and from the river leads to the formation of two distinct zones of denitrification (Figure 2, right column). The first one is located directly at the river-aquifer interface. It is active only at the times when flow is from the river into the aquifer, hence supplying nitrate. We estimated the maximum penetration depth of the river water by integrating the positive part of the

velocity function over one period. Via advection only, the water penetrates 0.23 m into the aquifer. Oxygen and nitrate reach that point only at very low concentrations because they are rapidly depleted after entering the aquifer.

The second zone of denitrification at about 1.1 m is fed by nitrate from the incoming groundwater. At the aquifer boundary, denitrification is mainly limited by carbon availability, such that nitrate concentrations remain at high values until the distance to the river is $x \approx 1.5$ m, after which they sharply decrease. Due to the flow reversal, this denitrification zone shifts between 1 m and 1.35 m over time. The response of concentrations to the dynamic flow is generally similar to the bank-filtration scenario where the dynamics are caused by fluctuating oxygen concentrations. Both solute concentrations and mRNA strongly fluctuate over time while enzyme concentrations and biomass are stable because of their longer time scales of production and decay.

Compared to the other two scenarios, the DOC concentration in the bank-storage scenario is high in the 1.2 m adjacent to the river. On average, the magnitude of the advective velocity is smaller in this scenario. This reduces the incoming mass flux of electron acceptors (nitrate and oxygen) in comparison to the other scenarios as the electron-acceptor concentrations remain the same. Additionally, more organic carbon can be released into each water parcel due to the longer residence time. Both effects lead to the overall higher DOC concentration. This highlights that the flow velocity is an important control on the carbon availability and thus microbial reaction kinetics in groundwater.

3.2. Impact of Model-Parameter Values

Our sensitivity analysis identified influential parameters via a PCA of local parameter sensitivities. In all scenarios, the first principal component explains nearly all of the variance in the parameter sensitivities (groundwater discharge: 97.7%, bank filtration: 91.3%, bank storage: 85%, see Figure S5 in Supporting Information S1). Only a few parameters contribute to the first component in all scenarios: The concentrations of nitrate in the inflowing groundwater and river water, the concentrations of oxygen and DOC in the river water, as well as the parameters related to carbon release from the matrix (see Figure S6 in Supporting Information S1).

Based on the PCA, we created an alternative parameter set by perturbing the reference parameters according to the weight w_j given to each parameter j in the first principal component (Figure S6 in Supporting Information S1). The perturbed parameter p_j^* is given by

$$p_j^* = p_j \exp(h\, w_j), \tag{23}$$

where h is a scaling factor.

A negative value of h produces a parameter set that increases the carbon availability in the system compared to the reference parameters and decreases the nitrate input into the system. Since the reactive system is strongly limited by carbon availability when using the reference parameter values, we chose to perturb the parameters toward a less carbon-limited system. We computed the concentration distributions and reaction rates with the alternative parameter set using $h = -2$ for the groundwater-discharge scenario. The perturbed parameters range between 0.2 and 2.5 times the reference parameters.

The spatial distributions of simulated concentrations using the alternative parameter sets are shown in Figure S7 in Supporting Information S1. Spatial and temporal patterns are generally similar to the ones in the simulations based on the reference parameters (Figure 2), but the perturbed parameters lead to a shift in the reaction zone. For example, denitrification in the groundwater-discharge scenario directly starts when the groundwater enters the domain. Transcript and enzyme concentrations are the highest between $x = 4$ m and $x = 2.5$ m.

3.3. Relationship Between Transcripts/Enzymes and Reaction Rates

Based on our simulation results, we computed denitrification rates to explore how transcript and enzyme concentrations relate to the denitrification activity in the different scenarios (see Figure 3 for transcripts and Figure S4 in Supporting Information S1 for enzymes).

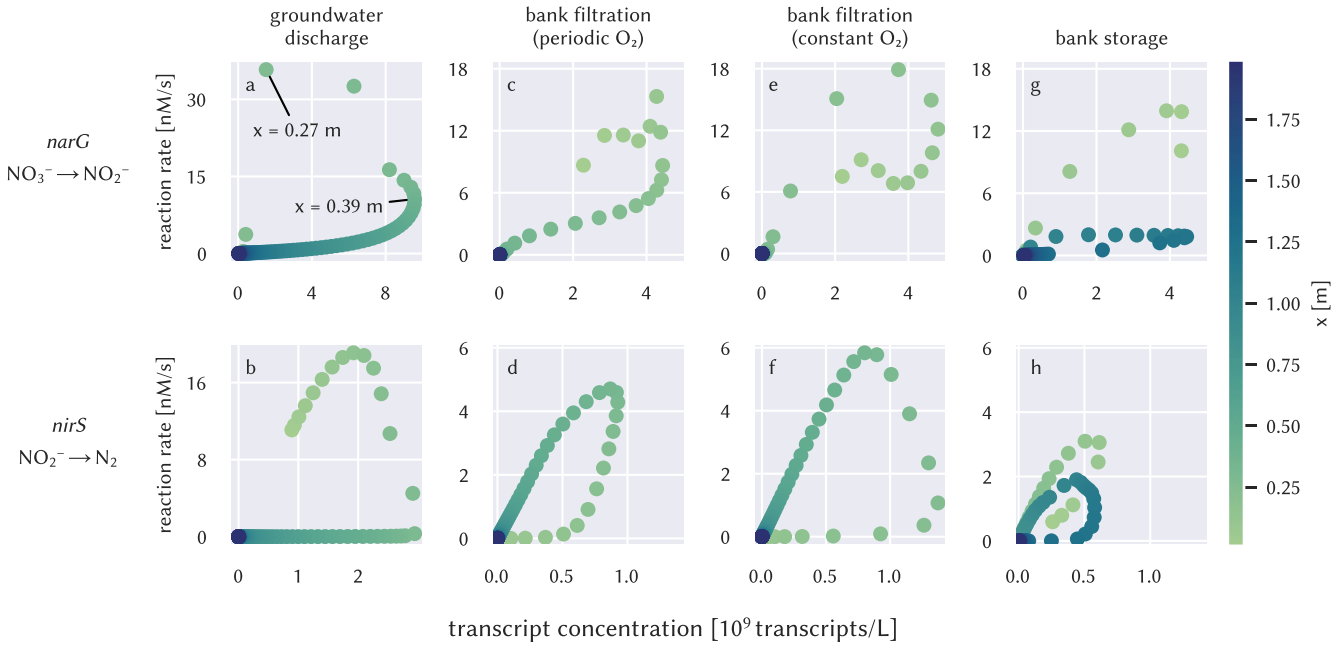

Figure 3. Relationships between the concentrations of functional-gene transcripts *narG* (upper row) and *nirS* (lower row) with the denitrification rates in the different scenarios. In the scenarios, where concentrations do not reach constant steady-state values but exhibit repeating diurnal cycles, daily averages of rates, and concentrations are shown. The color indicates the spatial coordinate with dark blue corresponding to the groundwater-inflow boundary and light green corresponding to the river boundary. Note that the axis scales are different for the groundwater-discharge scenario.

3.3.1. Scenario Groundwater Discharge

In the groundwater-discharge scenario, the system reaches a steady state where the enzyme concentrations are proportional to transcript concentrations. Therefore, it is sufficient to analyze the relationship between reaction rates and transcripts *or* enzymes. For simplicity, we compare rates to transcripts in Figures 3a and 3b. The relationships between rates and transcripts are nonlinear and the correlation is positive in some parts of the domain, but negative or zero in other parts. At the groundwater-inflow boundary (dark blue colors), both *narG* transcript concentrations and NO_3^- reduction rates are close to zero and increase toward the river (lighter colors). However, when the rates reach 10 nmol L^{-1} s^{-1} at 0.39 m, the trend reverses, i.e., where transcript levels decrease reaction rates increase and reach their maximum at 0.27 m. At the points closest to the river boundary, both the nitrate reduction rate and *narG* transcript levels return to zero, closing the hysteresis loop.

The concentrations of *nirS* transcripts rise between 1 and 0.3 m (Figure 3b). However, their increase does not correspond to an increase in reaction rates, suggesting that under certain conditions, transcript concentrations, and reaction rates may be completely decoupled. One may intuitively expect that increasing reaction rates would be accompanied by increasing transcript concentrations. However, the rise of reaction rates between 0.3 and 0.17 m is concomitant with the opposite, a decrease in transcript concentrations. A positive correlation between *nirS* transcript concentrations and reaction rates is only observed in the 15 cm closest to the river. The strong nonlinearity of the transcript-rate relationships (and partly negative correlations) can be explained by the limited availability of DOC over most of the domain (which in this scenario originates from the river and hydrolysis of POC). The latter limits denitrification, whereas transcript production is still triggered by the presence of nitrate and nitrite, irrespective of electron-donor availability.

3.3.2. Scenario Bank Filtration

Figures 4a and 4c show the relationship between transcript concentrations and denitrification rates for the bank-filtration scenario with a fluctuating oxygen inflow concentration. Reaction rates and transcript concentrations (and, to a smaller extent, also enzyme concentrations) both fluctuate over the course of the day, but the signals have a phase shift. This leads to a hysteresis in the relationship between transcript concentrations and reaction rates, with a different hysteretic pattern at different locations. Overall, transcript concentrations and denitrification rates do not show a clear (linear) relationship. These results suggest that it may not be possible to

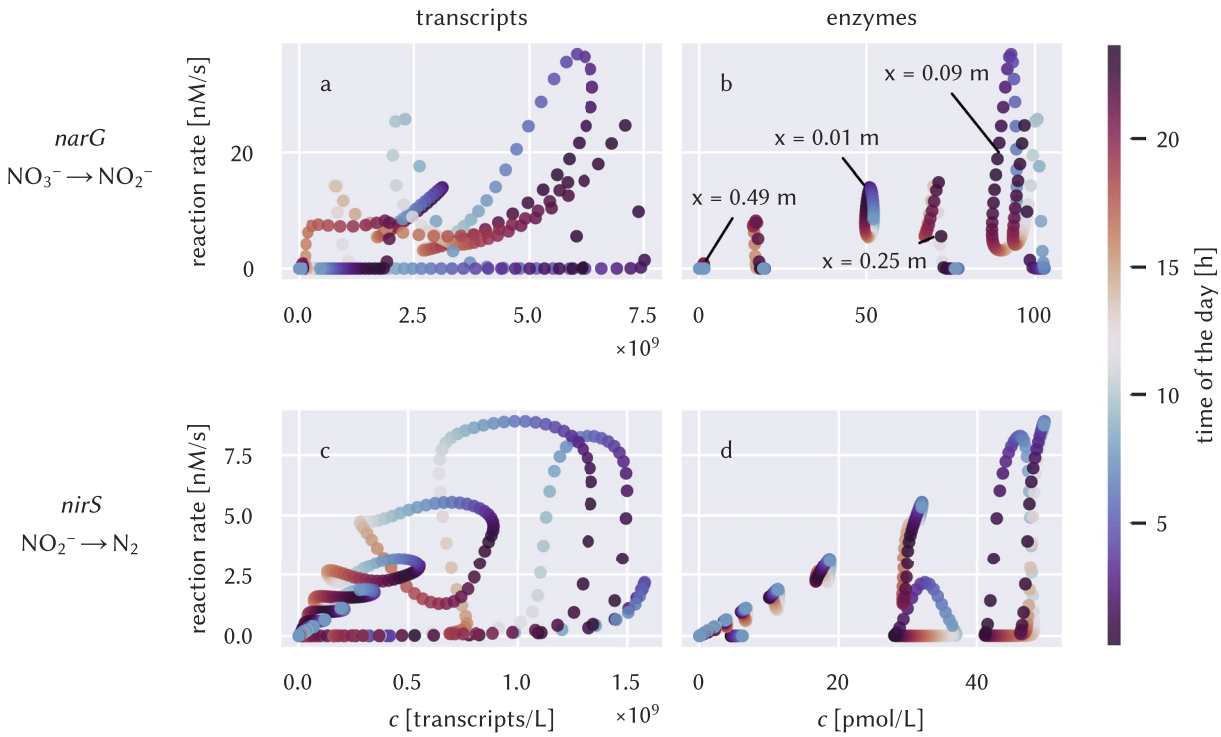

Figure 4. Relationships of transcript (left column) and enzyme (right column) concentrations with denitrification rates for the bank-filtration scenario where river water with fluctuating oxygen concentrations infiltrates groundwater. Colors indicate the time point within the diurnal cycle. Every point *x* in space shows a distinct pattern (with one "loop" corresponding to one point in space), and many of them are nonlinear and hysteretic in time.

infer the denitrification activity at a given time and location from determining the transcript concentration at a single time point.

The relationship between enzyme concentrations and denitrification rates (Figures 4b and 4d) is also highly nonlinear and location-specific. However, it exhibits less pronounced hysteresis loops because, in contrast to transcripts, the characteristic times for enzyme production and decay are longer than the time scale of the fluctuations. As a consequence, in dynamic steady state with diurnal cycles, the enzyme concentrations remain almost constant throughout the day, whereas the reaction rates fluctuate in response to the periodic concentration changes of aqueous substrates. Thus, enzyme distributions could, under the right conditions, be used as proxies for delineating the average denitrification activity.

For the mitigation of nitrate contamination in groundwater daily averages of reaction rates are of greater interest than their diurnal fluctuations. To investigate whether repeated transcript measurements could be used as indicators of denitrification activity, we compare the daily averages of the denitrification rates and the transcript concentrations in Figures 3c and 3d. As can be seen, upon averaging more distinct positive correlations emerge, although they are still nonunique, particularly in the case of *nirS* transcripts, where the same transcript concentration can be associated with rates that differ by more than 1 order of magnitude. Different combinations of nitrite, oxygen, and DOC concentrations can lead to the same transcript concentration, while the factors describing substrate limitation and oxygen inhibition affecting denitrification rates differ. The relationship looks very similar for transcripts and enzymes because daily averages of transcript concentrations are almost proportional to enzyme concentrations (see Figure S2 in Supporting Information S1).

The relationship between steady-state transcript concentrations and denitrification rates for the bank-filtration scenario with constant oxygen input (Figures 3e and 3f) slightly differs from the bank-filtration scenario with periodic oxygen concentrations (Figures 3c and 3d), but essentially mirrors its characteristic features. For example, both bank-filtration scenarios yield a positive, but nonunique, relationship of narG transcripts with the rates, whereas *nirS* transcripts exhibit a strong hysteretic behavior. It is to be expected that the relationships are generally similar for the steady-state solution and daily averages of the periodic solution as the simulated concentration

profiles are nearly the same in both cases (Figure 2, center), but nonlinearity in the rate laws can lead to the observed differences.

3.3.3. Scenario Bank Storage

Similar to the bank-filtration scenario with periodic oxygen concentration in the inflow, the periodic reversal of flow in the bank-storage scenario results in complex relationships between the transcript or enzyme concentrations and the denitrification rates (Figure S3 in Supporting Information S1). However, in contrast to the bank-filtration scenario with periodic oxygen concentration, daily averages of transcript concentrations and reaction rates (Figures 3g and 3h) show two clearly distinct patterns, corresponding to the two denitrification zones, and resembling to some extent the patterns of the pure groundwater-discharge and pure bank-filtration scenarios. In both zones, the relationships are nonlinear and nonunique, analogous to all other scenarios. This is most evident for the *narG* transcripts (shown in Figure 3d).

4. Discussion

4.1. Comparison of the Transcript-Rate Relationship Between Scenarios

We compared the relationship between transcript concentrations and reaction rates between the different scenarios to evaluate how biogeochemical and hydrological conditions affect the relationship according to the three scenarios. Transcript concentrations and reactions rates differed between the scenarios. For example, we observed that *narG* transcript concentrations are highest in the groundwater-discharge scenario, driven by the higher nitrate concentrations in the groundwater in comparison to the river water in the bank-filtration scenarios. In the bank-storage scenario, transcript concentrations are lower because microorganisms receive nitrate input only half of the time. While the exact absolute differences (e.g., in the slope or exact shape of the curve, or in magnitudes of reaction rates and transcript concentrations) are dependent on the choice of parameters and are hence site-specific, several general trends emerge.

Two patterns are common to all scenarios; they arise from the general system behavior and corresponding model structure, not from individual parameter values. First, we observe that in both dynamic scenarios time-shifts between the dynamics of transcripts and reactions yield a complex relationship between transcript concentrations and reaction rates. Averaging transcript concentrations over 1 day significantly simplifies the relationship in both cases (compare Figures 4 and 3). Even though this temporal uncoupling also depends on the values of reaction parameters that dictate the response times of transcripts and enzymes, the uncertainty of these parameters is relatively small in comparison to other parameters such as the half-saturation constants, where literature values range over several orders of magnitude (García-Ruiz et al., 1998). Typical time scales for the response time of transcripts and enzymes are on the order of minutes and hours, respectively (Bernstein et al., 2002; Maier et al., 2011). The second common pattern is that the relationship between (average) transcript concentrations and reaction rates is strongly nonlinear and nonunique. This is the case because, at least in our model, transcription also occurs under nonideal conditions, i.e., when reaction rates are limited by substrate availability or oxygen inhibition. Different combinations of limiting and inhibiting conditions at different locations produce the spatial hysteresis patterns.

Figure S8 in Supporting Information S1 shows the relationships between transcript concentrations and reaction rates obtained with the alternative parameter sets that we generated by perturbing sensitive parameters. Even though the exact shape of the relationship differs from the one obtained with the reference parameter values (compare Figure 3) both cases share the same qualitative features. The relationship between transcripts and denitrification rates is strongly nonlinear and hysteretic in space. The similar trends obtained after perturbing sensitive model parameters in comparison to the original parameter set provides confidence in the robustness of our parameters and the transferability of our model-based findings.

4.2. Unraveling the Relationship Between Transcript Concentrations and Reaction Rates

The relationships between transcript concentrations and denitrification reaction rates, presented in Section 3.3, clearly show that transcript concentrations are not a reliable predictor of denitrification rates, even in cases where these are proportional to enzyme concentrations. Deviations from an expected linear relationship arise because denitrification rates are not only limited by enzyme concentrations (which, in turn, are ultimately determined by

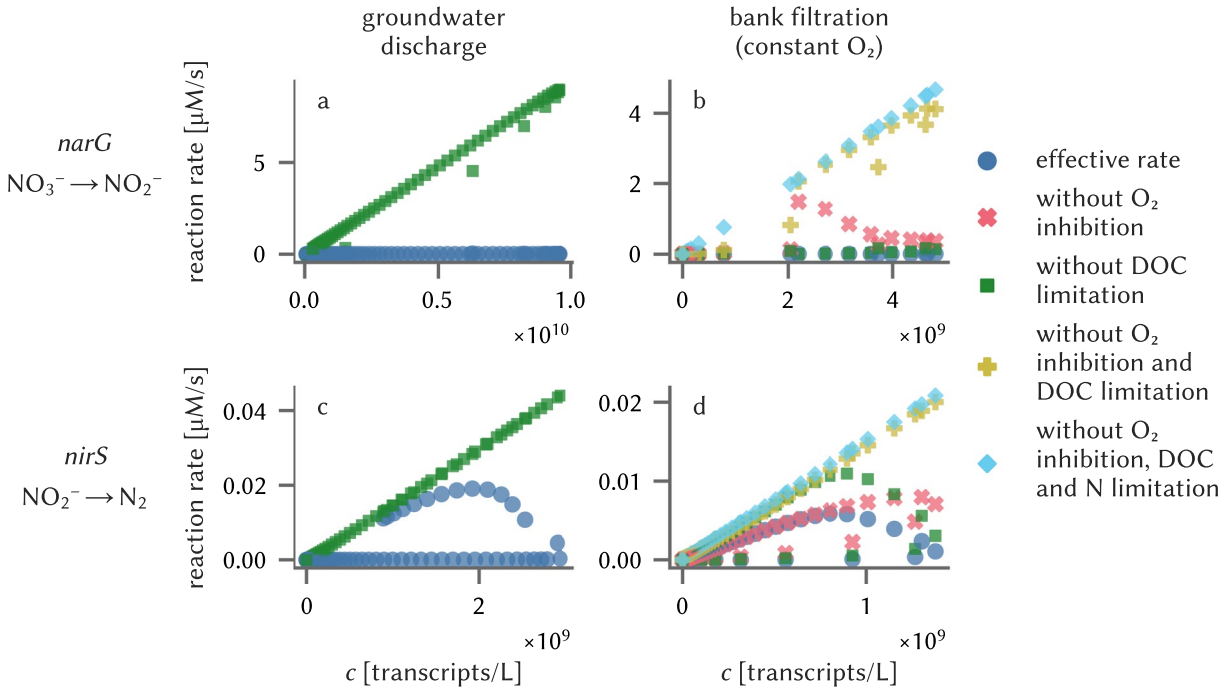

Figure 5. Relationship between the concentrations of functional-gene transcripts *narG* (upper row) and *nirS* (lower row) with potential denitrification rates after removing the effects of O_2 inhibition, dissolved organic carbon (DOC) limitation, nitrogen substrate limitation, or combinations thereof. (Note: Scenarios where concentrations do not reach a steady state are omitted because correcting for the rate limitations based on time-averaged concentrations is not a valid approach).

the nitrogen species triggering transcription), but also by substrate availability (in our study DOC and nitrogen species) and oxygen inhibition. In the following, we refer to the denitrification rates under in situ conditions that are limited by substrate availability and oxygen inhibition as the *effective* rates. In the model, we can eliminate these limitations by dividing the rate by the corresponding Michaelis-Menten or inhibition term, resulting in what we denote as *potential* denitrification rates. We performed this analysis successively with an increasing number of limitation terms, yielding a series of different potential rates. When these potential rates are compared to the transcript concentrations, clear positive relationships emerge (Figure 5).

In the groundwater-discharge scenario (Figures 5a and 5c), removing the DOC limitation yields a nearly linear relationship, highlighting that carbon limitation is the most important rate-limiting factor in this scenario. The remaining nonlinearity of *narG* transcripts at low reaction rates can be explained by the presence of nitrite near the river boundary, triggering *narG* transcription even though nitrate levels and thus nitrate-removal rates are low.

The current model assumes that transcription of the denitrification genes is independent of DOC availability. While this approach is consistent with the current understanding of the targeted regulation of denitrification genes by nitrogen species and oxygen (Gaimster et al., 2018), our model formulation neglects unspecific mechanisms of gene regulation that act to shut down microbial metabolism at low carbon availability, thereby affecting denitrification genes. Accounting for transcription downregulation of the denitrification genes under carbon limitation in our model formulation would likely yield relationships between transcripts and reaction rates closer to the potential rates without DOC limitation (Figure 5). Nonlinear effects of DOC limitation on the reaction rates would persist. However, the absolute deviation from a linear relationship would be negligible when transcript concentrations and, therefore, potential rates are close to zero. Under extreme electron-donor limitation, our model predicts very low absolute transcript concentrations even without explicitly accounting for DOC-controlled downregulation of transcription because DOC-limitation restricts microbial growth, leading to low biomass and, thereby, low transcript concentrations. However, if there is evidence for a large abundance of inactive denitrifiers, the model might need to distinguish between the active and an inactive microbial pool, in which transcription is shut off (e.g., Chavez Rodriguez et al., 2020).

In the case of bank filtration with a constant oxygen concentration (Figures 5b and 5d), accounting for the DOC limitation term alone does not remove the nonlinearity because oxygen inhibition also exerts an important control on denitrification. Eliminating both DOC limitation and oxygen inhibition leads to an approximately linear relationship between transcripts and potential rates. However, the potential rates are orders of magnitude larger than the effective (substrate-limited and inhibited) reaction rates.

In the scenarios in which concentrations undergo periodic fluctuations in time (bank filtration with period oxygen in the inflow and bank storage), applying the correction terms would only be permissible for the time-variable rates and concentrations, but not for the averages. This is because the correction terms are nonlinear and the concentrations involved are strongly correlated in time. Under such conditions, the product of their time-averaged values is not the same as the time average of their product. Hence, applying corrections to the time-averaged rates to obtain a more unique relationship of the time-averaged transcript concentrations is not permissible. Similar effects have been described for spatial correlations of degrader communities and substrate concentrations in carbon cycling models. Chakrawal et al. (2020) used scale-transition theory to analyze how spatial correlations among state variables or between state variables and kinetic parameters affect upscaled reaction rates. In theory, the same method could be applied to obtain time-averaged rates based on average concentrations. However, it requires knowing the covariance terms of substrate and enzyme concentrations in time, which is not possible in practice because highly time-resolved measurements of transcript or substrate (DOC, nitrogen species) concentrations in groundwater are not available in the first place.

4.3. Capturing Transcript Signatures in the Field

Our simulations show that transcripts of denitrification genes respond to short-term (diurnal) fluctuations of electron-acceptor concentrations, yielding highly temporally variable transcript concentrations at the river-groundwater interface. In such a dynamic system, analyses based on transcripts of functional genes would strongly depend on the time point of sampling. Transcripts exhibiting a low, even undetectable, abundance at a given time, may be present at much higher concentrations at other times of the day, and vice versa. Hence, interpretations on overall system behavior based on transcript concentrations obtained from sporadic sampling events, could be misleading in highly dynamic biogeochemical environments such as those found at the river-groundwater interface.

Based on our modeling results, we simulated transcript measurements over time and space to illustrate, how different sampling frequencies and times can affect the outcome captured by measurement campaigns. Figure 6a shows time series of *nirS* transcript concentrations in the bank-filtration scenario with fluctuating oxygen concentrations at a distance of 0.17 m from the river, sampled at different frequencies (weekly samples, daily samples, 3 and 10 samples per day). We added a small random time perturbation to the sampling times to represent a realistic situation. The high sampling frequency of 10 samples per day captures the diurnal signal quite well. Taking 3 samples per day also captures the dynamic behavior of the system, albeit with less accuracy, with many of the peaks cut off and an apparent signal that is more irregular than then true one. Daily and weekly sampling creates apparent patterns in the data that are not linked to any real process but that are due to sampling the diurnal signal at slightly different times each day or week.

Figure 6b shows a spatial profile of simulated transcript measurements, taken at two different times of the day. While the general shape of the two profiles is similar, the location of the peak is shifted by about 10 cm, and between 5 cm and 20 cm the concentrations between the two time points differ by up to 2 orders of magnitude. This example emphasizes the need to consider the relevant time scale of variation for transcripts when planning measurement campaigns. When transcription is regulated by redox-active species such as nitrate and oxygen (as is the case for denitrification), simple tools like redox-sensitive or oxygen-sensitive probes could provide a first approximation of what the relevant time scale for transcript dynamics is and guide the sampling frequency accordingly.

4.4. Implications for the Design of Field Sampling and Measurements

In contrast to transcripts, the concentrations of functional enzymes and functional biomass (which can be estimated by functional-gene concentrations) are much more dampened and hardly respond to diurnal fluctuations of electron-acceptor availability because of the longer time scales of their production and decay, as discussed in

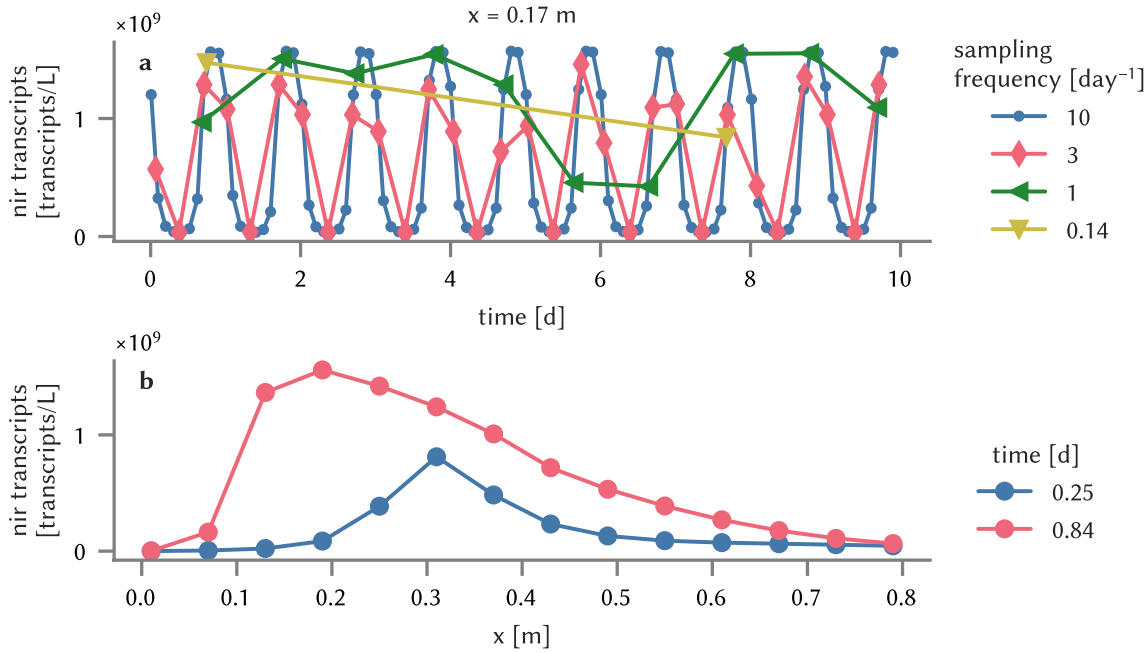

Figure 6. Simulated measurements of the *nirS* transcript concentrations in the bank-filtration scenario with fluctuating oxygen concentrations. (a) Effect of different sampling frequencies on a time series measured at a fixed location ($x = 0.17$ m). (b) Dependence of a spatial profile on the time of the measurement.

Section 3.1.2. As a consequence, DNA-based methods such as the quantification of functional genes or metagenomics can provide information less dependent on short-term fluctuations of electron-acceptor or electron-donor concentrations. However, a DNA-based approach, analogous to an enzyme-based approach, is subject to other uncertainties related to DNA's persistence and presence outside of active organisms (relic DNA) that can distort the characterization of the microbial community (Carini et al., 2016; Lennon et al., 2018; Nielsen et al., 2007), an effect not considered in this study. Different approaches to filter out the signals from relic DNA (viability PCR, e.g., Carini et al., 2016; Fittipaldi et al., 2012) and inactive microbes (BONCAT-FACS, selecting for translationally active cells, e.g., Couradeau et al., 2019) have been developed in the past years but are not yet applied routinely.

The unresponsiveness of enzyme concentrations and biomass in a system with short-term dynamics also implies that incorporating their time-variability into a biogeochemical model is not necessary and they can be assumed to be constant in time (i.e., via a biomass-implicit rate formulation). However, spatial variations should be considered, e.g., by using spatially variable rate coefficients. In systems in which the concentrations of electron acceptors vary over larger time scales (seasonal dynamics, flood events with effects of several days), the temporal variability of functional biomass and particularly enzyme concentrations might also play a role. Measurements of functional enzymes would also provide a more robust picture of microbial activity compared to functional-gene transcripts, because they are less affected by short-term fluctuations. Unfortunately, the quantification of functional enzymes (as opposed to transcripts) is not yet an established measurement technique for environmental samples, even though some pioneering studies have been performed (e.g., Li et al., 2017a).

Daily averaged transcript concentrations, however, are proportional to enzyme concentrations (for the scenarios investigated here), thus implying that several transcript measurements in time could replace the more difficult to measure enzymes in groundwater systems. Because only averages are required, mixing samples from several time points prior to RNA extraction could also help to reduce transcript measurement efforts. The main challenge, however, lies in obtaining samples from the same location at several time points, as sampling for gene quantification is destructive. When reactions are much slower than advective transport (low Damköhler number), several samples along a flow path at a single time point (representing water parcels infiltrated at different times) could replace samples from the same location at several time points. In our simulations, however, reactions deplete substrates within a few centimeters. Water parcels with a time difference of 12 hr are separated by a distance of 0.43 m, such that averaging over the locations does not provide a replacement for the temporal average at a single

location. Therefore, samples should be taken at adjacent locations, corresponding to the same distance along a flow path (which would be made more difficult by heterogeneity). The latter illustrates the difficulty of acquiring time-resolved field measurements of transcripts. However, column experiments in the laboratory that simulate conditions in the field (see, e.g., Liu et al., 2017) provide a potential alternative, and would be a useful addition to capture higher-resolution dynamics.

Even after time averaging, transcript or enzyme concentrations are not reliable predictors of reactions rates. The relationships in the simulated scenarios are nonunique and nonlinear. Our analysis reveals that enzyme concentrations can be interpreted as a proxy for *potential* rates, which are hypothetical rates in the absence of specific limitations, such as substrate limitation and oxygen inhibition. These limitations reduce the potential rates toward the *effective* (in-situ) reaction rates.

Based on these findings we argue that an approach to predict denitrification rates directly from transcript or enzyme data would need to account for the challenges outlined, necessitating the following steps: As a first step, the relationship between transcript concentrations and potential reaction rates needs to be determined. This could be achieved with lab incubations under nonlimiting conditions. A caveat here is that under nonlimiting conditions, a different part of the microbial community with a different physiology might be more active than under in-situ conditions (Hazard et al., 2021), modifying the relationship. In a system at steady state the relationship between transcript concentrations and potential reaction rates should ideally be linear. Measured transcript concentrations can subsequently serve as a predictor of potential rates which then need to be amended by rate-limiting factors like substrate limitation to obtain the effective reaction rates. This correction step does not only require measurements of the involved solute concentrations, but also estimates of parameters describing rate-limiting factors of reaction kinetics (half-saturation and inhibition constants). Such parameter values are often not well known and reported values typically range over several orders of magnitude (see, e.g., García-Ruiz et al., 1998). Therefore, additional experiments to determine specific parameters of the studied system would be necessary.

Extending process-based reactive-transport models to simulate molecular-biological data provides a powerful integrative approach to predict reaction rates from concentrations and molecular-biological data. Upon calibration to all available data, such a process-based model can deliver reaction rates at time points and locations where no data are available. We therefore suggest the following strategy of combining molecular-biological data, biogeochemical measurements, and modeling to determine denitrification rates.

1. *Measure functional enzymes, genes, or transcripts to determine temporally stable, spatial profiles of the active functional biomass*: Our simulations show that profiles of daily averaged transcript concentrations, enzymes, and functional biomass are very similar and may generally be linked to the denitrification activity. Given the challenges of measuring time averages of transcript concentrations and excluding inactive biomass in DNA-based methods, enzyme measurements seem to be the most accurate proxy variable for active functional biomass. These data will provide a relative measure of the spatially variable maximum rate coefficient in a biomass-implicit rate formulation. Compared to an enzyme-explicit formulation (as used in this study), a biomass-implicit formulation has the advantage that it requires fewer parameters. The hypothesis that the active functional biomass maintains a constant spatial distribution should be verified with repeated measurements at different time points, and seasonal trends could be accounted for by using season-dependent rate coefficients. If a considerable time-variability of active functional biomass is observed, a biomass-explicit or enzyme-explicit model formulation that provides a process-based explanation for the variability should replace the biomass-implicit formulation.
2. *Measure oxygen, nitrogen substrates, and DOC at several locations with a high temporal resolution*: These data are required to appropriately account for substrate limitations and oxygen inhibition. The required resolution depends on the typical length and time scales of the system and might need to be determined iteratively. Spatial gradients and dominant temporal dynamics should be resolved. To capture the short-term variability inherent to these variables, continuous logging with probes, if possible, is a good approach (e.g., for oxygen). Otherwise, manual measurements should also cover several temporal scales. For example, hourly measurements that capture diurnal dynamics on individual days could be combined with daily or weekly samples to provide information about longer-term dynamics.
3. *Use a process-based model to obtain temporally and spatially resolved predictions of concentrations and reaction rates*: The model integrates the different data types through the calibration of model parameters,

yielding estimates of total in-situ denitrification rates, that are otherwise impossible to obtain with direct measurements.

The predictions of a reactive-transport model strongly depend on transport related parameters, such as flow velocities or solute fluxes at boundaries, governed by subsurface hydraulic conductivity. Therefore, at field sites, complementary hydrogeological data should accompany biogeochemical investigations. For example, natural-tracer and artificial-tracer studies can provide information on travel times and the average flow velocity. If flow cannot reasonably be assumed to be uniform and one-dimensional, hydraulic head data at several locations and aquifer tests to obtain hydraulic conductivity (e.g., slug tests) are required to set up a groundwater flow model.

5. Conclusions

Our model exercise highlights some of the prospects and limitations of using functional-gene transcripts and enzymes to characterize biogeochemical reactions at the river-groundwater interface. Concentrations of functional-gene transcripts quickly respond to changes in substrate concentrations and oxygen levels, implying that dynamic systems need to be sampled at the appropriate temporal resolution. High transcript and enzyme concentrations spatially coincide with active processes (here, denitrification) and are therefore qualitative indicators of reactive zones. Substrate limitation and oxygen inhibition of the enzymes, however, lead to complex, nonunique relationships between transcript or enzyme concentrations and reaction rates. Admittedly, our model only considers one part of the subsurface nitrogen cycle in detail (i.e., gene regulation of denitrification). The advantage is that it enables a relatively straightforward analysis of the resulting patterns. However, even then, the model predicts the emergence of complex relationships between transcript or enzyme concentrations and the denitrification rate. Thus, we caution against the use of concentrations of functional-gene transcripts and enzymes as direct proxies of microbial reaction rates.

Our results highlight that a rigorous quantitative interpretation of transcript or enzyme data requires a process-based mathematical model that is able to reflect nonlinear interactions between biogeochemical processes and the regulation of gene and enzyme abundances. While our purely numerical study provides predictions of expected transcript and enzyme behavior in dynamic natural systems, it does not replace laboratory and field investigations. In fact, we emphasize that further improvements in enzyme-explicit models should go hand-in-hand with the acquisition of highly temporally resolved data that enable us to interrogate and calibrate the models.

The general, qualitative conclusions from our analysis should be transferable to other microbial reaction systems in environmental settings. Soils, for instance, are a very dynamic environment where redox conditions can change abruptly through changes in hydrological conditions like drainage or flooding (Pronk et al., 2020; Zhang & Furman, 2021). Such short-term fluctuations will lead to a disconnect of quickly reacting transcript concentrations from enzyme concentrations and, consequently, reaction rates. Additionally, oxygen availability in soils can vary spatially over very short distances because the slow diffusion of oxygen into the matrix produces anoxic microsites (Zhang & Furman, 2021). The spatial hysteresis patterns that our model predicts for larger spatial gradients of oxygen and nitrogen species (centimeter to meters) might then occur on very small spatial scales (millimeters).

In many environmental or engineered systems, other nitrogen-cycling processes (e.g., nitrification, annamox, DNRA), alternative electron donors (e.g., reduced sulfur and iron species/minerals), and the temperature dependence of the reaction kinetics can all affect denitrification rates. Incorporating parallel and competing processes to the current version of our model will likely be necessary to capture nitrogen reaction dynamics at any particular site. In addition to modifying the spatial and temporal distributions of concentrations and reaction rates, this may also change the transcript-rate relationships. However, we expect that the general features that we observed—time-variable nonlinear and nonunique relationships—will remain valid.

Acronyms

BDF	Backwards Differentiation Formula
DNRA	Dissimilatory nitrate reduction to ammonium
DOC	Dissolved organic carbon

NAR	Nitrate reductase
NIR	Nitrite reductase
ODE	Ordinary differential equation
POC	Particulate organic carbon

Data Availability Statement

Version 0.2.0 of the Python package Nitrogene (Störiko et al., 2022) used for defining the reaction model and analyzing output data is preserved at https://doi.org/10.5281/zenodo.6584591, available under an MIT license and developed openly at https://gitlab.com/astoeriko/nitrogene. The repository also contains the output data used to generate figures. Version 0.2.0 of the Python package adrpy (Störiko, 2022) used for coupling the reactions to 1-D advective-dispersive transport is preserved at https://doi.org/10.5281/zenodo.6584641, available under an MIT license and developed openly at https://gitlab.com/astoeriko/adrpy. Version 0.2.2 of the Sunode library (Seyboldt, 2021) used to solve the ODEs resulting from spatial discretization of the advection-dispersion-reaction equation is preserved at https://doi.org/10.5281/zenodo.5213947, available under an MIT license and developed openly at https://github.com/aseyboldt/sunode.

Acknowledgments
This work was funded by the German Research Foundation (DFG) within the Research Training Group RTG 1829 Integrated Hydrosystem Modelling (DFG Grant agreement GRK 1829) and the Collaborative Research Center CRC 1253 CAMPOS-Catchments as Reactors, project P7 (DFG Grant agreement SFB 1253/1). The authors thank three anonymous reviewers for their valuable and constructive feedback. Open access provided through Projekt DEAL.

References

Akbarzadeh, Z., Laverman, A. M., Rezanezhad, F., Raimonet, M., Viollier, E., Shafei, B., & Van Cappellen, P. (2018). Benthic nitrite exchanges in the Seine River (France): An early diagenetic modeling analysis. *Science of the Total Environment*, *628–629*, 580–593. https://doi.org/10.1016/j.scitotenv.2018.01.319

Anantharaman, K., Brown, C. T., Hug, L. A., Sharon, I., Castelle, C. J., Probst, A. J., et al. (2016). Thousands of microbial genomes shed light on interconnected biogeochemical processes in an aquifer system. *Nature Communications*, *7*, 13219. https://doi.org/10.1038/ncomms13219

Bælum, J., Chambon, J. C., Scheutz, C., Binning, P. J., Laier, T., Bjerg, P. L., & Jacobsen, C. S. (2013). A conceptual model linking functional gene expression and reductive dechlorination rates of chlorinated ethenes in clay rich groundwater sediment. *Water Research*, *47*(7), 2467–2478. https://doi.org/10.1016/j.watres.2013.02.016

Bernstein, J. A., Khodursky, A. B., Lin, P.-H., Lin-Chao, S., & Cohen, S. N. (2002). Global analysis of mRNA decay and abundance in Escherichia coli at single-gene resolution using two-color fluorescent DNA microarrays. *Proceedings of the National Academy of Sciences of the United States of America*, *99*(15), 9697–9702. https://doi.org/10.1073/pnas.112318199

Bertin, C., & Bourg, A. C. M. (1994). Radon-222 and chloride as natural tracers of the infiltration of river water into an alluvial aquifer in which there is significant river/groundwater mixing. *Environmental Science & Technology*, *28*(5), 794–798. https://doi.org/10.1021/es00054a008

Bol, R., Lücke, A., Tappe, W., Kummer, S., Krause, M., Weigand, S., et al. (2015). Spatio-temporal variations of dissolved organic matter in a German forested mountainous headwater catchment. *Vadose Zone Journal*, *14*(4), vzj2015.01.0005. https://doi.org/10.2136/vzj2015.01.0005

Brow, C. N., O'Brien Johnson, R., Johnson, R. L., & Simon, H. M. (2013). Assessment of anaerobic toluene biodegradation activity by *bssA* transcript/gene ratios. *Applied and Environmental Microbiology*, *79*(17), 5338–5344. https://doi.org/10.1128/AEM.01031-13

Carini, P., Marsden, P. J., Leff, J. W., Morgan, E. E., Strickland, M. S., & Fierer, N. (2016). Relic DNA is abundant in soil and obscures estimates of soil microbial diversity. *Nature Microbiology*, *2*(3), 16242. https://doi.org/10.1038/nmicrobiol.2016.242

Chakrawal, A., Herrmann, A. M., Koestel, J., Jarsjö, J., Nunan, N., Kätterer, T., & Manzoni, S. (2020). Dynamic upscaling of decomposition kinetics for carbon cycling models. *Geoscientific Model Development*, *13*(3), 1399–1429. https://doi.org/10.5194/gmd-13-1399-2020

Chavez Rodriguez, L., Ingalls, B., Schwarz, E., Streck, T., Uksa, M., & Pagel, H. (2020). Gene-centric model approaches for accurate prediction of pesticide biodegradation in soils. *Environmental Science & Technology*, *54*(21), 13638–13650. https://doi.org/10.1021/acs.est.0c03315

Couradeau, E., Sasse, J., Goudeau, D., Nath, N., Hazen, T. C., Bowen, B. P., et al. (2019). Probing the active fraction of soil microbiomes using BONCAT-FACS. *Nature Communications*, *10*(1), 2770. https://doi.org/10.1038/s41467-019-10542-0

Ding, D. (2010). Transport of bacteria in aquifer sediment: Experiments and modeling. *Hydrogeology Journal*, *18*(3), 669–679. https://doi.org/10.1007/s10040-009-0559-3

Fittipaldi, M., Nocker, A., & Codony, F. (2012). Progress in understanding preferential detection of live cells using viability dyes in combination with DNA amplification. *Journal of Microbiological Methods*, *91*(2), 276–289. https://doi.org/10.1016/j.mimet.2012.08.007

Gaimster, H., Alston, M., Richardson, D. J., Gates, A. J., & Rowley, G. (2018). Transcriptional and environmental control of bacterial denitrification and N_2O emissions. *FEMS Microbiology Letters*, *365*(5), fnx277. https://doi.org/10.1093/femsle/fnx277

García-Ruiz, R., Pattinson, S. N., & Whitton, B. A. (1998). Kinetic parameters of denitrification in a river continuum. *Applied and Environmental Microbiology*, *64*(7), 2533–2538. https://doi.org/10.1128/AEM.64.7.2533-2538.1998

Gelhar, L. W., Welty, C., & Rehfeldt, K. R. (1992). A critical review of data on field-scale dispersion in aquifers. *Water Resources Research*, *28*(7), 1955–1974. https://doi.org/10.1029/92WR00607

Gerecht, K. E., Cardenas, M. B., Guswa, A. J., Sawyer, A. H., Nowinski, J. D., & Swanson, T. E. (2011). Dynamics of hyporheic flow and heat transport across a bed-to-bank continuum in a large regulated river. *Water Resources Research*, *47*, W03524. https://doi.org/10.1029/2010WR009794

Griebler, C., Mindl, B., Slezak, D., & Geiger-Kaiser, M. (2002). Distribution patterns of attached and suspended bacteria in pristine and contaminated shallow aquifers studied with an in situ sediment exposure microcosm. *Aquatic Microbial Ecology*, *28*(2), 117–129. https://doi.org/10.3354/ame028117

Grösbacher, M., Eckert, D., Cirpka, O. A., & Griebler, C. (2018). Contaminant concentration versus flow velocity: Drivers of biodegradation and microbial growth in groundwater model systems. *Biodegradation*, *29*(3), 211–232. https://doi.org/10.1007/s10532-018-9824-2

Gu, C., Hornberger, G. M., Mills, A. L., Herman, J. S., & Flewelling, S. A. (2007). Nitrate reduction in streambed sediments: Effects of flow and biogeochemical kinetics. *Water Resources Research*, *43*, W12413. https://doi.org/10.1029/2007WR006027

Härtig, E., & Zumft, W. G. (1999). Kinetics of *nirS* expression (cytochrome cd_1 nitrite reductase) in *Pseudomonas stutzeri* during the transition from aerobic respiration to denitrification: Evidence for a denitrification-specific nitrate- and nitrite-responsive regulatory system. *Journal of Bacteriology*, *181*(1), 161–166. https://doi.org/10.1128/JB.181.1.161-166.1999

Harvey, J. W., Böhlke, J. K., Voytek, M. A., Scott, D., & Tobias, C. R. (2013). Hyporheic zone denitrification: Controls on effective reaction depth and contribution to whole-stream mass balance. *Water Resources Research*, *49*, 6298–6316. https://doi.org/10.1002/wrcr.20492

Hassan, J., Bergaust, L. L., Wheat, I. D., & Bakken, L. R. (2014). Low probability of initiating *nirS* transcription explains observed gas kinetics and growth of bacteria switching from aerobic respiration to denitrification. *PLoS Computational Biology*, *10*(11), e1003933. https://doi.org/10.1371/journal.pcbi.1003933

Hassan, J., Qu, Z., Bergaust, L. L., & Bakken, L. R. (2016). Transient accumulation of NO_2^- and N_2O during denitrification explained by assuming cell diversification by stochastic transcription of denitrification genes. *PLoS Computational Biology*, *12*(1), e1004621. https://doi.org/10.1371/journal.pcbi.1004621

Hayashi, M., Vogt, T., Mächler, L., & Schirmer, M. (2012). Diurnal fluctuations of electrical conductivity in a pre-alpine river: Effects of photosynthesis and groundwater exchange. *Journal of Hydrology*, *450–451*, 93–104. https://doi.org/10.1016/j.jhydrol.2012.05.020

Hazard, C., Prosser, J. I., & Nicol, G. W. (2021). Use and abuse of potential rates in soil microbiology. *Soil Biology and Biochemistry*, *157*, 108242. https://doi.org/10.1016/j.soilbio.2021.108242

Hindmarsh, A. C., Brown, P. N., Grant, K. E., Lee, S. L., Serban, R., Shumaker, D. E., & Woodward, C. S. (2005). SUNDIALS: Suite of nonlinear and differential/algebraic equation solvers. *ACM Transactions on Mathematical Software*, *31*(3), 363–396. https://doi.org/10.1145/1089014.1089020

Kennedy, C. D., Genereux, D. P., Corbett, D. R., & Mitasova, H. (2009). Spatial and temporal dynamics of coupled groundwater and nitrogen fluxes through a streambed in an agricultural watershed. *Water Resources Research*, *45*, W09401. https://doi.org/10.1029/2008WR007397

Kinzelbach, W., Schäfer, W., & Herzer, J. (1991). Numerical modeling of natural and enhanced denitrification processes in aquifers. *Water Resources Research*, *27*(6), 1123–1135. https://doi.org/10.1029/91WR00474

Knights, D., Sawyer, A. H., Barnes, R. T., Musial, C. T., & Bray, S. (2017). Tidal controls on riverbed denitrification along a tidal freshwater zone. *Water Resources Research*, *53*, 799–816. https://doi.org/10.1002/2016WR019405

Koutinas, M., Kiparissides, A., Silva-Rocha, R., Lam, M.-C., Martins dos Santos, V. A. P., de Lorenzo, V., et al. (2011). Linking genes to microbial growth kinetics—An integrated biochemical systems engineering approach. *Metabolic Engineering*, *13*(4), 401–413. https://doi.org/10.1016/j.ymben.2011.02.001

Krause, S., Hannah, D. M., Fleckenstein, J. H., Heppell, C. M., Kaeser, D., Pickup, R., et al. (2011). Inter-disciplinary perspectives on processes in the hyporheic zone. *Ecohydrology*, *4*(4), 481–499. https://doi.org/10.1002/eco.176

Krause, S., Lewandowski, J., Grimm, N. B., Hannah, D. M., Pinay, G., McDonald, K., et al. (2017). Ecohydrological interfaces as hot spots of ecosystem processes. *Water Resources Research*, *53*, 6359–6376. https://doi.org/10.1002/2016WR019516

Kunz, J. V., Hensley, R., Brase, L., Borchardt, D., & Rode, M. (2017). High frequency measurements of reach scale nitrogen uptake in a fourth order river with contrasting hydromorphology and variable water chemistry (Weiße Elster, Germany). *Water Resources Research*, *53*, 328–343. https://doi.org/10.1002/2016WR019355

Kuypers, M. M. M., Marchant, H. K., & Kartal, B. (2018). The microbial nitrogen-cycling network. *Nature Reviews Microbiology*, *16*(5), 263–276. https://doi.org/10.1038/nrmicro.2018.9

Lennon, J. T., Muscarella, M. E., Placella, S. A., & Lehmkuhl, B. K. (2018). How, when, and where relic DNA affects microbial diversity. *mBio*, *9*(3), e00637-18. https://doi.org/10.1128/mBio.00637-18

Li, M., Gao, Y., Qian, W.-J., Shi, L., Liu, Y., Nelson, W. C., et al. (2017). Targeted quantification of functional enzyme dynamics in environmental samples for microbially mediated biogeochemical processes. *Environmental Microbiology Reports*, *9*(5), 512–521. https://doi.org/10.1111/1758-2229.12558

Li, M., Qian, W.-J., Gao, Y., Shi, L., & Liu, C. (2017). Functional enzyme-based approach for linking microbial community functions with biogeochemical process kinetics. *Environmental Science & Technology*, *51*(20), 11848–11857. https://doi.org/10.1021/acs.est.7b03158

Liu, Y., Liu, C., Nelson, W. C., Shi, L., Xu, F., Liu, Y., et al. (2017). Effect of water chemistry and hydrodynamics on nitrogen transformation activity and microbial community functional potential in hyporheic zone sediment columns. *Environmental Science & Technology*, *51*(9), 4877–4886. https://doi.org/10.1021/acs.est.6b05018

Louca, S., Hawley, A. K., Katsev, S., Torres-Beltran, M., Bhatia, M. P., Kheirandish, S., et al. (2016). Integrating biogeochemistry with multiomic sequence information in a model oxygen minimum zone. *Proceedings of the National Academy of Sciences of the United States of America*, *113*(40), E5925–E5933. https://doi.org/10.1073/pnas.1602897113

Maier, T., Schmidt, A., Güell, M., Kühner, S., Gavin, A.-C., Aebersold, R., & Serrano, L. (2011). Quantification of mRNA and protein and integration with protein turnover in a bacterium. *Molecular Systems Biology*, *7*, 511. https://doi.org/10.1038/msb.2011.38

Mailloux, B. J., & Fuller, M. E. (2003). Determination of in situ bacterial growth rates in aquifers and aquifer sediments. *Applied and Environmental Microbiology*, *69*(7), 3798–3808. https://doi.org/10.1128/AEM.69.7.3798-3808.2003

Marmonier, P., Fontvieille, D., Gibert, J., & Vanek, V. (1995). Distribution of dissolved organic carbon and bacteria at the interface between the Rhône River and its alluvial aquifer. *Journal of the North American Benthological Society*, *14*(3), 382–392. https://doi.org/10.2307/1467204

McDonough, L. K., Santos, I. R., Andersen, M. S., O'Carroll, D. M., Rutlidge, H., Meredith, K., et al. (2020). Changes in global groundwater organic carbon driven by climate change and urbanization. *Nature Communications*, *11*(1), 1279. https://doi.org/10.1038/s41467-020-14946-1

Mellage, A., Eckert, D., Grösbacher, M., Inan, A. Z., Cirpka, O. A., & Griebler, C. (2015). Dynamics of suspended and attached aerobic toluene degraders in small-scale flow-through sediment systems under growth and starvation conditions. *Environmental Science & Technology*, *49*(12), 7161–7169. https://doi.org/10.1021/es5058538

Monard, C., Martin-Laurent, F., Lima, O., Devers-Lamrani, M., & Binet, F. (2013). Estimating the biodegradation of pesticide in soils by monitoring pesticide-degrading gene expression. *Biodegradation*, *24*(2), 203–213. https://doi.org/10.1007/s10532-012-9574-5

Moran, M. A., Satinsky, B., Gifford, S. M., Luo, H., Rivers, A., Chan, L.-K., et al. (2013). Sizing up metatranscriptomics. *The ISME Journal*, *7*(2), 237–243. https://doi.org/10.1038/ismej.2012.94

Nielsen, K. M., Johnsen, P. J., Bensasson, D., & Daffonchio, D. (2007). Release and persistence of extracellular DNA in the environment. *Environmental Biosafety Research*, *6*(1–2), 37–53. https://doi.org/10.1051/ebr:2007031

Pronk, G. J., Mellage, A., Milojevic, T., Smeaton, C. M., Engel, K., Neufeld, J. D., et al. (2020). Carbon turnover and microbial activity in an artificial soil under imposed cyclic drainage and imbibition. *Vadose Zone Journal*, *19*(1), e20021. https://doi.org/10.1002/vzj2.20021

Qu, Z., Bakken, L. R., Molstad, L., Frostegård, Å., & Bergaust, L. L. (2015). Transcriptional and metabolic regulation of denitrification in *Paracoccus denitrificans* allows low but significant activity of nitrous oxide reductase under oxic conditions. *Environmental Microbiology*, *18*(9), 2951–2963. https://doi.org/10.1111/1462-2920.13128

Rahm, B. G., & Richardson, R. E. (2008). *Dehalococcoides* ' gene transcripts as quantitative bioindicators of tetrachloroethene, trichloroethene, and *cis*-1,2-dichloroethene dehalorespiration rates. *Environmental Science & Technology*, *42*(14), 5099–5105. https://doi.org/10.1021/es702912t

Ramkrishna, D., & Song, H.-S. (2019). *Cybernetic modeling for bioreaction engineering*. Cambridge University Press. https://doi.org/10.1017/9780511731969

Reid, T., Chaganti, S. R., Droppo, I. G., & Weisener, C. G. (2018). Novel insights into freshwater hydrocarbon-rich sediments using metatranscriptomics: Opening the black box. *Water Research*, *136*, 1–11. https://doi.org/10.1016/j.watres.2018.02.039

Rocca, J. D., Hall, E. K., Lennon, J. T., Evans, S. E., Waldrop, M. P., Cotner, J. B., et al. (2015). Relationships between protein-encoding gene abundance and corresponding process are commonly assumed yet rarely observed. *The ISME Journal*, *9*(8), 1693–1699. https://doi.org/10.1038/ismej.2014.252

Rohe, L., Oppermann, T., Well, R., & Horn, M. A. (2020). Nitrite induced transcription of *p450nor* during denitrification by *Fusarium oxysporum* correlates with the production of N_2O with a high ^{15}N site preference. *Soil Biology and Biochemistry*, *151*, 108043. https://doi.org/10.1016/j.soilbio.2020.108043

Sanz-Prat, A., Lu, C., Amos, R. T., Finkel, M., Blowes, D. W., & Cirpka, O. A. (2016). Exposure-time based modeling of nonlinear reactive transport in porous media subject to physical and geochemical heterogeneity. *Journal of Contaminant Hydrology*, *192*, 35–49. https://doi.org/10.1016/j.jconhyd.2016.06.002

Sawyer, A. H. (2015). Enhanced removal of groundwater-borne nitrate in heterogeneous aquatic sediments. *Geophysical Research Letters*, *42*, 403–410. https://doi.org/10.1002/2014GL062234

Sawyer, A. H., Cardenas, M. B., Bomar, A., & Mackey, M. (2009). Impact of dam operations on hyporheic exchange in the riparian zone of a regulated river. *Hydrological Processes*, *23*(15), 2129–2137. https://doi.org/10.1002/hyp.7324

Scheidegger, A. E. (1974). *The physics of flow through porous media* (3rd ed.). University of Toronto Press. https://doi.org/10.3138/9781487583750

Seyboldt, A. (2021). Sunode. [Software]. Zenodo. https://doi.org/10.5281/zenodo.5213947

Simon, J., & Klotz, M. G. (2013). Diversity and evolution of bioenergetic systems involved in microbial nitrogen compound transformations. *Biochimica et Biophysica Acta (BBA)-Bioenergetics*, *1827*(2), 114–135. https://doi.org/10.1016/j.bbabio.2012.07.005

Smith, H. J., Zelaya, A. J., De León, K. B., Chakraborty, R., Elias, D. A., Hazen, T. C., et al. (2018). Impact of hydrologic boundaries on microbial planktonic and biofilm communities in shallow terrestrial subsurface environments. *FEMS Microbiology Ecology*, *94*(12), fiy191. https://doi.org/10.1093/femsec/fiy191

Song, H.-S., Thomas, D. G., Stegen, J. C., Li, M., Liu, C., Song, X., et al. (2017). Regulation-structured dynamic metabolic model provides a potential mechanism for delayed enzyme response in denitrification process. *Frontiers in Microbiology*, *8*, 1866. https://doi.org/10.3389/fmicb.2017.01866

Stelzer, R. S., Bartsch, L. A., Richardson, W. B., & Strauss, E. A. (2011). The dark side of the hyporheic zone: Depth profiles of nitrogen and its processing in stream sediments. *Freshwater Biology*, *56*(10), 2021–2033. https://doi.org/10.1111/j.1365-2427.2011.02632.x

Stief, P., Beer, D., & Neumann, D. (2002). Small-scale distribution of interstitial nitrite in freshwater sediment microcosms: The role of nitrate and oxygen availability, and sediment permeability. *Microbial Ecology*, *43*(3), 367–377. https://doi.org/10.1007/s00248-002-2008-x

Stoliker, D. L., Repert, D. A., Smith, R. L., Song, B., LeBlanc, D. R., McCobb, T. D., et al. (2016). Hydrologic controls on nitrogen cycling processes and functional gene abundance in sediments of a groundwater flow-through lake. *Environmental Science & Technology*, *50*(7), 3649–3657. https://doi.org/10.1021/acs.est.5b06155

Störiko, A. (2022). Adrpy: Advection-Dispersion-Reaction models in Python. [Software]. Zenodo. https://doi.org/10.5281/zenodo.6584641

Störiko, A., Pagel, H., Mellage, A., & Cirpka, O. (2022). Nitrogene: Modelling code and data of an enzyme-based denitrification model. [Software]. Zenodo. https://doi.org/10.5281/zenodo.6584591

Störiko, A., Pagel, H., Mellage, A., & Cirpka, O. A. (2021). Does it pay off to explicitly link functional gene expression to denitrification rates in reaction models? *Frontiers in Microbiology*, *12*, 684146. https://doi.org/10.3389/fmicb.2021.684146

Thurman, E. M. (1985). *Organic geochemistry of natural waters (No. 2)*. Springer. https://doi.org/10.1007/978-94-009-5095-5

Wang, S., Wang, W., Zhao, S., Wang, X., Hefting, M. M., Schwark, L., & Zhu, G. (2019). Anammox and denitrification separately dominate microbial N-loss in water saturated and unsaturated soils horizons of riparian zones. *Water Research*, *162*, 139–150. https://doi.org/10.1016/j.watres.2019.06.052

Wegner, C.-E., Gaspar, M., Geesink, P., Herrmann, M., Marz, M., & Küsel, K. (2019). Biogeochemical regimes in shallow aquifers reflect the metabolic coupling of the elements nitrogen, sulfur, and carbon. *Applied and Environmental Microbiology*, *85*(5), e02346-18. https://doi.org/10.1128/AEM.02346-18

Zhang, Z., & Furman, A. (2021). Soil redox dynamics under dynamic hydrologic regimes—A review. *Science of the Total Environment*, *763*, 143026. https://doi.org/10.1016/j.scitotenv.2020.143026